HHS Public Access

Author manuscript

Sci Transl Med. Author manuscript; available in PMC 2017 October 19.

Published in final edited form as:

Sci Transl Med. 2016 October 19; 8(361): 361ra139. doi:10.1126/scitranslmed.aaf5504.

NAD+ repletion improves muscle function in muscular dystrophy and counters global PARylation

Dongryeol Ryu[1,*], **Hongbo Zhang**[1,*], **Eduardo R. Ropelle**[1,2,*], **Vincenzo Sorrentino**[1], **Davi A. G. Mázala**[3], **Laurent Mouchiroud**[1], **Philip L. Marshall**[4], **Matthew D. Campbell**[5], **Amir Safi Ali**[5], **Gary M. Knowels**[5], **Stéphanie Bellemin**[6], **Shama R. Iyer**[7], **Xu Wang**[1], **Karim Gariani**[1], **Anthony A. Sauve**[8], **Carles Cantó**[9], **Kevin E. Conley**[5], **Ludivine Walter**[6], **Richard M. Lovering**[7], **Eva R. Chin**[3,†], **Bernard J. Jasmin**[10], **David J. Marcinek**[5], **Keir J. Menzies**[1,4,‡], and **Johan Auwerx**[1,‡]

[1]Laboratory of Integrative and Systems Physiology, École Polytechnique Fédérale de Lausanne, 1015 Lausanne, Switzerland [2]Laboratory of Molecular Biology of Exercise, School of Applied Science, University of Campinas, CEP 13484-350 Limeira, São Paulo, Brazil [3]Department of Kinesiology, School of Public Health, University of Maryland, College Park, MD 20742, USA [4]Interdisciplinary School of Health Sciences, University of Ottawa Brain and Mind Research Institute and Centre for Neuromuscular Disease, Ottawa, Ontario K1H 8M5, Canada [5]Department of Radiology, University of Washington, Seattle, WA 98195, USA [6]Centre de Génétique et de Physiologie Moléculaires et Cellulaires, Université Claude Bernard Lyon 1, CNRS UMR 5534, 69622 Villeurbanne, France [7]Department of Orthopaedics, University of Maryland School of Medicine, Baltimore, MD 21201, USA [8]Department of Pharmacology, Weill Cornell Medical School, New York, NY 10065, USA [9]Nestlé Institute of Health Sciences, 1015 Lausanne, Switzerland [10]Department of Cellular and Molecular Medicine and Centre for Neuromuscular Disease, Faculty of Medicine, University of Ottawa, Ottawa, Ontario K1H 8M5, Canada

Abstract

Neuromuscular diseases are often caused by inherited mutations that lead to progressive skeletal muscle weakness and degeneration. In diverse populations of normal healthy mice, we observed correlations between the abundance of mRNA transcripts related to mitochondrial biogenesis, the dystrophin-sarcoglycan complex, and nicotinamide adenine dinucleotide (NAD^+) synthesis, consistent with a potential role for the essential cofactor NAD^+ in protecting muscle from metabolic and structural degeneration. Furthermore, the skeletal muscle transcriptomes of patients

‡Corresponding author. admin.auwerx@epfl.ch (J.A.); kmenzies@uottawa.ca (K.J.M.).
*These authors contributed equally to this work.
†Present address: Cytokinetics Inc., South San Francisco, CA 94080, USA.

Author contributions: D.R., H.Z., E.R.R., K.J.M., and J.A. conceived and designed the project. D.R., H.Z., E.R.R., V.S., D.A.G.M., L.M., P.L.M., M.D.C., A.S.A., G.M.K., S.B., S.R.I., X.W., K.G., A.A.S., C.C., K.E.C., L.W., R.M.L., E.R.C, B.J.J., D.J.M., and K.J.M. performed the experiments. K.J.M. and J.A. wrote the manuscript, with contributions from D.R. and H.Z.

Competing interests: C.C. is an employee of the Nestlé Institute of Health Sciences. A.A.S. is a founder and consultant of Metro MidAtlantic Biotech LLC, a company targeting NAD pathways for therapies. Cornell University and A.A.S. received royalties for sales of NR from Chroma Dex Inc., a company selling ingredients including NR. J.A. is a scientific founder and a science advisory board member of Mitobridge, which develops therapies for mitochondrial diseases.

Data and materials availability: Data and materials not presented in the article are available from the authors.

with Duchene's muscular dystrophy (DMD) and other muscle diseases were enriched for various poly[adenosine 5'-diphosphate (ADP)–ribose] polymerases (PARPs) and for nicotinamide *N*-methyltransferase (NNMT), enzymes that are major consumers of NAD^+ and are involved in pleiotropic events, including inflammation. In the *mdx* mouse model of DMD, we observed significant reductions in muscle NAD^+ levels, concurrent increases in PARP activity, and reduced expression of nicotinamide phosphoribosyltransferase (NAMPT), the rate-limiting enzyme for NAD^+ biosynthesis. Replenishing NAD^+ stores with dietary nicotinamide riboside supplementation improved muscle function and heart pathology in *mdx* and *mdx/Utr*$^{-/-}$ mice and reversed pathology in *Caenorhabditis elegans* models of DMD. The effects of NAD^+ repletion in *mdx* mice relied on the improvement in mitochondrial function and structural protein expression (α-dystrobrevin and δ-sarcoglycan) and on the reductions in general poly(ADP)-ribosylation, inflammation, and fibrosis. In combination, these studies suggest that the replenishment of NAD^+ may benefit patients with muscular dystrophies or other neuromuscular degenerative conditions characterized by the *PARP/NNMT* gene expression signatures.

INTRODUCTION

Muscular dystrophies result from a reduction in the muscle cell support network that connects the myofilament proteins within the cell to the basal lamina outside the cell, rendering the sarcolemma more susceptible to damage. Caused by an X-linked mutation, Duchene's muscular dystrophy (DMD) affects 1 in 3500 males and often leads to death due to heart or respiratory failure (1, 2). The deterioration of muscle function and strength results from progressive muscle damage, fibrosis, and necrosis; there is no effective treatment. DMD symptoms are shared by other pathologies that involve muscle wasting, such as cancer, AIDS, and aging, which are all characterized by declines in metabolic and physiological parameters, with progressive weakness in skeletal muscle. Despite advances in exon skipping and other genetic and pharmacological approaches to treating DMD, the delivery, effectiveness, and safety of these therapies are not optimal (3), necessitating the development of other therapeutic strategies.

Recent studies have indicated that sirtuin 1 (SIRT1)–dependent mitochondrial biogenesis can reduce *mdx* mice pathology and muscle atrophy (4–7). Fatigue and muscle weakness, as seen in DMD, are also symptoms of mitochondrial myopathies and metabolic diseases [reviewed in (8)]. Nicotinamide adenine dinucleotide (NAD^+) repletion provides protection from metabolic diseases and mitochondrial dysfunction induced by diet or aging, often in a SIRT1-dependent manner (9–14). Sirtuins, in general, consume NAD^+ as a cofactor for the deacetylation of proteins while also generating nicotinamide (NAM). Similarly, poly[adenosine 5′-diphosphate (ADP)– ribose] polymerase (PARP) proteins consume NAD^+ during the poly(ADP)-ribosylation (PARylation) of proteins. As a result, PARP inhibition or genetic loss of function of *PARP1* in mice increases muscle NAD^+ levels and sirtuin-directed mitochondrial biogenesis (11, 15).

The initial evidence for the involvement of PARP activity in DMD was the increased PARP1 expression in 20 patient skeletal muscle biopsies, which was correlated with reduced telomere length (16). In addition, we recently demonstrated that NAD^+ repletion could delay

both age-related and *mdx* muscle stem cell senescence, although we did not analyze muscle function, PARP activation, or the link between NAD^+ metabolism and structural gene expression (17). NAD^+ promotes the polymerization of laminin and the subcellular localization of paxillin, an integrin-associated adaptor protein, improving cell adhesion in a zebrafish model of muscular dystrophy (18). From these independent lines of evidence, we hypothesized that NAD^+ availability—controlled, in part, by the conversion of NAM to nicotinamide mononucleotide (NMN) via the rate-limiting salvage enzyme nicotinamide phosphoribosyltransferase (NAMPT), by further conversion of NMN to NAD^+ by NMN adenylyltransferases (NMNATs), and by NAD^+ consumption by a panel of PARP proteins (Fig. 1A) [reviewed in (19)]—could have a multifaceted influence on the development of muscle weakness and fatigue in DMD and potentially other neuromuscular diseases (17).

RESULTS

Correlations between transcripts related to NAD^+ metabolism and muscular dystrophy

To evaluate the relationship between muscle NAD^+ metabolism and muscle health, we first examined the correlations between transcripts of NAD^+-salvagingor NAD^+-consuming enzymes and diverse muscle parameters. We assessed the natural variance in transcript abundance in quadriceps muscles of 42 strains of genetically diverse, healthy BXD mice (fig. S1, A and B) (20–22) and observed that *Nampt* and *Nmnat3* mRNA levels correlated with muscle mass (Fig. 1, B and C). *Nampt* mRNA levels also correlated with the expression of transcripts related to mitochondrial biogenesis (Fig. 1D). In custom-generated gene sets from the BXD mouse strains that expressed the highest and lowest levels of *Nampt* transcripts, genes related to mitochondrial biogenesis, autophagy, and muscle regeneration, along with *Nmnat1*, were also enriched (fig. S1C) (23). On the basis of this preliminary analysis, we performed a principal components analysis on these networks using all 42 BXD strains. In the resulting factor loading plot, transcripts encoding genes relating to mitochondrial biogenesis, the dystrophin-sarcoglycan complex, and muscle regeneration were strongly correlated to the expression of *Nampt, Nmnat1*, and *Nrk1* [an enzyme that converts nicotinamide riboside (NR) into NMN], consistent with a beneficial effect of NAD^+ synthesis on several aspects of muscle function (Fig. 1E). We then plotted a circular schematic using the same set of genes to demonstrate the positive and negative correlations among them (Fig. 1F). Genes associated with the pathogenesis of muscle dystrophy in *mdx* mice were individually negatively correlated with NAD^+ synthesis and mitochondrial biogenesis (related genes in this principal components analysis), whereas genes related to mitochondrial biogenesis and muscle structure and growth correlated positively. We then examined the expression of transcripts involved in NAD^+ homeostasis in extant human skeletal muscle data sets from patients with DMD in comparison to controls (24, 25). In contrast to a previously described elevation in *PARP1* expression in DMD muscle (16), we saw no change in *PARP1* expression but did discover a consistent enrichment of other *PARP* transcripts and of the nicotinamide *N*-methyltransferase (*NNMT*) transcript, an enzyme that shunts the NAD^+ precursor NAM away from NAD^+ biosynthesis through methylation (Fig. 1G) (26, 27). This *PARP/NNMT* gene signature was unexpectedly also seen in biopsies from patients with a large variety of muscular dystrophies or (neuro)muscular disease (fig. S2A). In contrast, expression of genes associated with NAD^+ biosynthesis was generally reduced

in these data sets (Fig. 1H and fig. S2B). These findings suggest that NAD^+ depletion occurs both in patients with DMD and in those with other (neuro)muscular diseases.

NAD^+ levels as a marker of elevated PARP activity in *mdx* mice

Given the central role of NAD^+ in mitochondrial homeostasis and organismal metabolism (28), we set out to determine whether reduced NAD^+ levels could explain the attenuation of mitochondrial function in the muscle of *mdx* mice and could be used as an in vivo marker of muscle damage. In vivo noninvasive ^{31}P magnetic resonance spectroscopy (MRS) measurements of NAD^+ levels were lower in *mdx* muscle than in controls (Fig. 2A). Reduced NAD^+ levels were also confirmed by mass spectrometry measurements (11) in postmortem muscle specimens from *mdx* muscles (Fig. 2B). Because PARP transcripts were expressed at a high level in muscles from DMD patients (Fig. 1G), we hypothesized that overactivation of PARPs could be responsible for the depletion of NAD^+ levels in *mdx* mice, an idea further bolstered by our recent data showing the contrasting situation of elevated NAD^+ levels in *Parp1* knockout mice (15) or in PARP inhibitor–treated mice (11). Consistent with our hypothesis, PARP protein levels were higher in *mdx* mice than in controls, including PARP1, PARP2, and PARP4 (fig. S2C), all of which have poly(ADP-ribose) polymerase activity. In addition, PARP activity and global protein PARylation levels were increased in *mdx* muscle (Fig. 2C), reinforcing the usefulness of the *mdx* model for comparisons to DMD. Global protein PARylation levels were also elevated in the muscle from *mdx/Utr*$^{-/-}$ double-mutant mice (fig. S2D). Furthermore, as predicted from the reduction in *Nampt* transcripts in human DMD patients (Fig. 1H), NAMPT protein levels were reduced in *mdx* muscle, potentially contributing to reductions in NAD^+ levels (Fig. 2D). Notably, NMNAT1 and NMNAT3 protein levels were not changed in *mdx* mice. These results indicate that *mdx*-induced damage is accompanied by PARP activation, attenuated NAD^+ salvage, and reduced NAD^+ levels, which may be potential markers of muscular dysfunction.

Limited NAD^+ affects in vivo energetics and mitochondrial function in *mdx* mice

To corroborate the known positive relationship between mitochondrial biogenesis and NAD^+ metabolism [reviewed in (19)], we assessed the mitochondrial energetics of skeletal hindlimb muscles from *mdx* mice using in vivo ^{31}P MRS to measure adenosine 5′-triphosphate (ATP) and phosphocreatine (PCr) fluxes (Fig. 2E). PCr buffers cellular ATP levels through the creatine kinase reaction. Therefore, the ratio of PCr/ ATP reflects the cellular energy state. Compared to control WT mice, the lower PCr/ATP ratio in the *mdx* hindlimb is a reflection of energy stress and demonstrates a greater load on the mitochondria to maintain ATP levels (Fig. 2F). This greater load on the mitochondria is also apparent in the relationship between resting and maximal mitochondrial ATP production. As reported in *mdx* mice (29), the maximum mitochondrial oxidative phosphorylation rate (ATP_{max}) was reduced in vivo compared to WT mice, whereas the resting adenosine triphosphatase (ATPase) activity, which reflects resting mitochondria ATP synthesis, was unchanged (Fig. 2F). Thus, *mdx* hindlimb mitochondria had to function at a greater fraction of their capacity to meet ATP demand (ATPase), than WT mitochondria, and were therefore under a greater energy stress (lower PCr/ATP). Explaining these energetic impairments and reaffirming the role of NAD^+ in the mitochondria, protein levels for both nuclear- and mitochondrial-

encoded proteins, including ATP5A, UQCRC2, MTCO1, SDHB, and TOM20, were lower in *mdx* mice than in controls (Fig. 2G). A lower abundance of complexes I, II, IV, and V in *mdx* skeletal muscles was also seen by blue native gel electrophoresis (Fig. 2H), and citrate synthase (CS) activity in *mdx* muscle extracts was reduced compared to control samples (Fig. 2I). Together, these data confirm that NAD^+ levels are attenuated in *mdx* muscles, resulting in impaired tissue energetics and mitochondrial function.

NR enhances muscle function in cells and in *dys-1;hlh-1* mutant *Caenorhabditis elegans*

Boosting NAD^+ levels with various NAD^+ precursors could potentially improve mitochondrial function and therefore muscle health (9, 30). To test this hypothesis, we evaluated the effects of the NAD^+ precursor NRon mitochondrial function in mouse C2C12 skeletal muscle cells. NR increased the NAD^+ levels in differentiated C2C12 myotubes (Fig. 3A), which elevated the mitochondrial complex abundance in a SIRT1-dependent manner, as evidenced by the use of the SIRT1 inhibitor EX527 (fig. S3A). NR also increased the maximal electron transport system capacity inC2C12 myotubes after exposure to the uncoupler FCCP (carbonyl cyanide *p*-trifluoromethoxyphenylhydrazone) (Fig. 3B). Consistent with the fact that the beneficial impact of NAD^+ boosting relies on sirtuin-mediated protein deacetylation, global protein acetylation was reduced in NR-treated C2C12 myotubes in a dose- and time-dependent fashion (Fig. 3C). Furthermore, NR modulated myotube mitochondrial protein expression and FOXO1 acetylation in a SIRT1-dependent fashion, as evidenced by pharmacological (using EX527) (Fig. 3D) and genetic (using a SIRT1 short hairpin RNA) SIRT1 loss-of-function experiments (fig. S3B). The induction of mitochondria-related transcripts after NR was also dependent on SIRT1, as demonstrated by the attenuation of the induction with EX527 (Fig. 3E).

We further investigated the involvement of SIRT1 in mediating the effect of NR by studying the mobility of worms carrying mutations for both the dystrophin-like gene *dys-1* and the MyoD homolog *hlh-1*; these worms display time-dependent impairments of locomotion and muscle degeneration during aging (31). By increasing NAD^+ levels (fig. S3C), NR improved the mobility of *dys-1;hlh-1* mutant worms over the course of 6 days of aging, an effect that was attenuated upon feeding worms with *sir-2.1* RNAi, which targeted the worm ortholog of SIRT1 (Fig. 3F). When this experiment was repeated with dead bacteria in the presence of NR, similar results were obtained (fig. S3D).We also examined whether *N*(1)-methylnicotinamide (mNAM), potentially generated from NR, could induce a mitohormetic signal by acting as a substrate for the ortholog of the mammalian aldehyde oxidase AOx1 gene GAD-3 to generate reactive oxygen species (32). However, two different concentrations of mNAM had no effect on *dys-1;hlh-1* worm movement (fig. S3E). We therefore conclude that mNAM production from NR is unlikely to explain the beneficial effects of NR on *dys-1;hlh-1* worms. After 8 days of NR treatment, there was also a *sir-2.1*–dependent improvement in worm paralysis (Fig. 3G). The *dys-1;hlh-1* worms exhibited less muscle degeneration when treated with NR (Fig. 3H). This favorable effect was lost with *sir-2.1* RNAi (Fig. 3H). Together, these results suggest that NR enhances mitochondrial function in C2C12 myotubes and improves mobility and the dystrophic phenotype in *C. elegans*, in a SIRT1-dependent manner.

NR reduces PARylation and improves in vivo muscle energetics in *mdx* mice

These data led us to test whether NR prevents or delays the onset of mitochondrial dysfunction in muscular dystrophy. Using a preventive approach, we fed chow diet supplemented with NR (400 mg/kg per day) to 4-week-old *mdx* mice for 12 weeks and assessed the NAD^+ levels and mitochondrial energetics in vivo with ^{31}P MRS. NR enhanced in vivo NAD^+ bioavailability in the hindlimb muscles (Fig. 4A), as well as in postmortem measurements performed on the gastrocnemius of *mdx* mice (Fig. 4B). NAD^+ levels were also lower in the livers of *mdx* mice and were restored by NR supplementation, whereas no change was observed in the NAD^+ levels in subcutaneous white adipose tissue (fig. S3, F and G). The increase in NAD^+ levels was concurrent with a reduction in PARP activity and global PARylation (Fig. 4C), as well as with elevated NAMPT, NMNAT1, and NMNAT3 protein expression, in *mdx* muscle (Fig. 4D). With unchanged ATP levels (Fig. 4E), NAD^+ repletion improved the PCr/ATP ratio, indicating less energy stress in NR-treated muscles. The reduced energy stress was confirmed by an elevation in the mitochondrial capacity (higher ATP_{max}) without changing the resting ATPase activity (Fig. 4F). Therefore, because NR-treated *mdx* mice exhibited a higher ATP_{max}, their hindlimb muscle mitochondria were able to work at a lower fraction of their capacity to meet ATP demand (ATPase) and were therefore under a lower energy stress (higher PCr/ATP). This was accompanied by increased abundance of individual oxidative phosphorylation proteins and of mitochondrial complexes II, IV, and V (Fig. 4, G and H). In addition, CS activity and cytochrome *c* oxidase histochemical staining were increased in NR-treated *mdx* gastrocnemius muscles (Fig. 4, I and J). As a result, NR treatment increased the running capacity in *mdx* mice (Fig. 4K), in the absence of body weight and lean mass differences (fig. S3, H and I). The respiratory exchange ratio was lower in *mdx* than in control mice, an effect that was surprisingly attenuated with NR (fig. S3J). Cardiac dysfunction has been reported in aged *mdx* mice (33). NR treatment decreased cardiac fibrosis and cardiomyocyte necrosis in 16-month-old *mdx* mice (Fig. 4, L and M). Thus, NR treatment effectively increased NAD^+ levels and corrected the mitochondrial profile of *mdx* animals, leading to in vivo improvements in muscle energetics and function.

NAD^+ repletion protects *mdx* muscle from damage, inflammation, and fibrosis

Because levels of the transcripts of the dystrophin-sarcoglycan complex and muscle regeneration are correlated with *Nampt, Nmnat1*, and *Nrk1* expression in the BXD reference population (Fig. 1, E and F), we next determined whether changes in NAD^+ altered muscle integrity in *mdx* mice. NR treatment in a preventive mode produced a robust increase in α-dystrobrevin and δ-sarcoglycan proteins in the gastrocnemius of *mdx* mice (Fig. 5A). Furthermore, NR-treated *mdx* mice were less susceptible to muscle damage, as shown by reduced permeability to Evans Blue (Fig. 5, B to D), decreased plasma creatine kinase levels (Fig. 5E), and increased grip strength (fig. S4A). Susceptibility to injury was reduced in *mdx* animals during repeated lengthening contractions, from a loss of 64% (SEM ± 15) to a 34% loss (SEM ± 12) upon NR treatment (Fig. 5F). The average minimal Feret's diameter, and corresponding distribution, showed an increase in fiber size with NR treatment in *mdx* mice (Fig. 5G and fig. S4B). This was confirmed in these same mice by quantifying the average and distribution of cross-sectional area of muscle fibers (Fig. 5, G and H, and fig. S4C). These mice also showed a reduced number of centralized nuclei in the tibialis anterior (TA)

muscles (Fig. 5H). In conjunction with the improved muscle function and the reduced muscle damage with NR, muscle inflammation was decreased in NR-treated *mdx* mice. This was reflected by the ability of NR treatment to reduce macrophage infiltration (fig. S4D) and to attenuate *Tnfα* transcript levels in the skeletal muscle of *mdx* mice (fig. S4E). The reduction of skeletal muscle inflammation by NR was also seen in the diaphragm, as demonstrated by reductions in staining for CD45 in transverse and longitudinal muscle sections (Fig. 5I and fig. S4F). After NR treatment, there was a reduction in acetylated p65 [nuclear factor κB (NF-κB)], a known deacetylation target of SIRT1 (34), leading us to further speculate that a reduction in NAD^+-dependent SIRT1 activity led to the improved inflammatory state of skeletal muscle in *mdx* mice (Fig. 5J). We also examined a population of muscle resident cells expressing mesenchymal platelet-derived growth factor receptor α (PDGFRα), capable of differentiating in vitro to fibrogenic or adipogenic lineages and named fibro/adipogenic precursors (FAPs) (35, 36), after NR treatment in *mdx* mice. The number of FAP cells is higher in both *mdx* and *mdx/Utr*$^{-/-}$ mice, causing the deposition of both skeletal muscle fat and connective tissues (37, 38). FAP cell numbers were lower both in the TA (fig. S4, G and H) and in transverse and longitudinal sections of the diaphragm (Fig. 5K and fig. S4, I and J) of *mdx* mice given an NR supplement. Similarly, NR treatment reduced the appearance of fibrosis in both transverse and longitudinal sections of the diaphragm of *mdx* mice (Fig. 5K and fig. S4K).

Because there are a larger number of inflammatory cells in *mdx* compared to in control muscle, we explored the major sites of PARylation by performing immunohistochemical stains of PARylated proteins and of CD45 on skeletal muscle sections. These stains exhibited minimal overlap, indicating that the PARylation of proteins occurred mostly in skeletal muscle nuclei (Fig. 5L). These predominantly myofiber nuclei further showed reduced PARylation upon NR treatment, as indicated by weaker nuclear staining intensity when compared to the $CD45^+$ hematopoietic cells (Fig. 5L and quantified in fig. S5).

We next tested whether NR would be effective in reversing muscle damage that had already taken place, a situation more therapeutically relevant. NR treatment for 5 to 7 weeks (starting at 3 weeks of age) in the more severe and already symptomatic *mdx/Utr*$^{-/-}$ double-mutant DMD mouse model induced phenotypic improvements similar to those seen in *mdx* mice. (We examined the reversal of degeneration in the *mdx/Utr*$^{-/-}$ mice because, unlike *mdx* mice, they do not show periods of spontaneous muscle regeneration.) The average and distribution of cross-sectional area and minimal Feret's diameter were all increased by NR treatment (Fig. 6, A to C, and fig. S6). Furthermore, grip strength was improved in *mdx/Utr*$^{-/-}$ mice with NR (Fig. 6D). These effects on skeletal muscle in *mdx/Utr*$^{-/-}$ mice were accompanied by similar improvements in the cardiac manifestations of the disease, as reflected by the reduction in cardiac fibrosis, necrosis, and inflammatory cell infiltration with NR treatment (Fig. 6E). This provides evidence that repletion of NAD^+ stores can slow and potentially reverse components of muscular dysfunction in two mouse models of muscular dystrophy.

DISCUSSION

We have demonstrated here that muscular dystrophy in *mdx* mice is associated with muscle NAD^+ depletion, which can potentially be monitored as an index of disease severity using ^{31}P MRS. Reduced NAD^+ levels are likely the result of PARP activation and reduced NAD^+ salvage (Fig. 4, A and C), as postulated from the robust *PARP/NNMT* gene enrichment signature that we observed in human dystrophy patients (Fig. 1G and fig. S2A). PARP activation was previously shown to be negatively correlated with energy expenditure; hence, reducing PARP activity improves metabolism by increasing intracellular NAD^+ levels (11, 15). NAD^+ repletion in different animal models of muscular dystrophy with NR exploits an alternative NAD^+ synthesis pathway to counter increased PARP consumption of NAD^+, leading to the recovery of NAD^+-dependent sirtuin signaling. This effect attenuates the loss of mitochondrial function and the susceptibility for muscle degeneration and necrosis in *mdx* and *mdx/Utr*$^{-/-}$ mice, which may in turn be responsible for the reduced requirement for global PARP activation (Fig. 6F). Despite elevations in NAD^+, there are reductions of global PARylation because PARP activity is dependent on various factors such as inflammation for activation, as has been shown in liver inflammation and fibrosis (39). Because inflammation is attenuated in *mdx* mice after NR treatment, we propose that this lowers the level of PARP activation in muscle, thus slowing the development of fibrosis. These data underscore the importance of NR as an alternative substrate for NAD^+ biosynthesis that can be exploited to increase muscle strength and decrease susceptibility to mechanical damage while reducing plasma creatine kinase levels and fibrosis. We also demonstrate the ability of NR to improve skeletal muscle strength and reduce cardiac fibrosis and inflammation in the more severe mouse model of DMD, *mdx/Utr*$^{-/-}$ mice. Our previous data showed that NR can help rejuvenate senescent muscle stem cells from both aged and *mdx* mice (17), and this may also be a contributing factor to the overall benefit of NR on *mdx* muscle function.

Our study therefore demonstrates that the use of NR and, potentially, other NAD^+ precursors, such as NMN and nicotinic acid (NA) analogs, and/or inhibitors of NAD^+ consumption, such as PARP inhibitors, could be effective for managing the progression of muscular dystrophy. All these compounds have been shown to improve respiratory capacity in diet- or age-related mitochondrial dysfunction (11, 12, 40) and to reduce inflammation (41–43). Finally, these data confirm the importance of SIRT1 as a target for treating the *mdx* phenotype (4) and for preventing FOXO-directed muscle degeneration (7, 44). Our observations may have broad implications for other neuromuscular diseases, injuries, or forms of muscle degeneration that are characterized by mitochondrial dysfunction or general PARP activation.

MATERIALS AND METHODS

Study design

The primary objective of this study was to investigate the use of NR to restore NAD^+ levels in response to the overactivation of the PARP family of proteins in various animal models of muscle degenerative disease. In vivo studies included cohorts of *mdx* and *mdx/Utr*$^{-/-}$ mice and *dys-1(cx18);hlh-1(cc561ts)* double-mutant *C. elegans* and existing transcriptomic data from patient muscle samples with various neuromuscular diseases (24, 25). Cell culture

studies used the C2C12 mouse myoblast cell line to explore the structural and metabolic effects of NAD^+ boosting strategies.

The sample size was estimated on the basis of the known variability of the assay, and for mouse studies, we were guided by the results obtained according to the standard operational procedures, established and validated within the EUMORPHIA program (45). All mouse experiments were performed once. Mice that showed any sign of severity, predefined by the Veterinary Office of the Canton of Vaud, Switzerland (authorization no. 2665), were euthanized. These animals, together with those who died spontaneously during the experiments, were excluded from the data analyses. These criteria were established before starting the experiments. Outliers not following the normal distribution of the samples were removed based on Grubb's test. For all experiments in *C. elegans*, the sample size was based on the known variability of the assay determined as described (55). All experiments, except when mentioned, were done in a non-blinded manner.

Animal experiments

Three-week-old male C57BL/10SnJ or C57BL/10ScSn-*Dmd*^{mdx}/J (The Jackson Laboratory) mice were fed with control or NR diet (triflate salt, custom-synthesized at 99% purity by NovAliX SA; 400 mg/kg per day) for 8 weeks beginning at 3.5 weeks of age. The *mdx/Utr*$^{-/-}$ double-mutant strain was generated by crossing C57BL/10ScSn-*Dmd*^{mdx}/J with *Utrn*^{tm1Ked}/J mice (The Jackson Laboratory). Experiments with *mdx/Utr*$^{-/-}$ mice included both male and females fed with control or NR diet (400 mg NR/kg mouse weight per day) up to 13 weeks, beginning at 3.5 weeks of age. Each pelleted diet was prepared as described previously (17). Most clinical tests were carried out according to standard operational procedures established and validated within the EUMORPHIA program (45). Body composition was determined by EchoMRI (Echo Medical Systems), and oxygen consumption (VO_2), food intake, and activity levels were monitored during the indirect calorimetry tests using the Comprehensive Laboratory Animal Monitoring System (Columbus Instruments) after 3 weeks of treatment. After 5 weeks of NR treatment, the grasp strength of four limbs was measured (Columbus Instruments); this was repeated four times with 5-min intervals. Endurance capacity was performed as published (46, 47) after 7 weeks of treatment. All animals were sacrificed after an overnight fast and 4- to 6-hour refed conditions. Blood was collected upon sacrifice, whereas tissues were collected, weighed, and flash-frozen in liquid nitrogen.

Ethical approval

These experiments were authorized by the Veterinary Office of the Canton of Vaud, Switzerland (authorization no. 2665).

Cell culture

The C2C12 mouse myoblast cell line was obtained from the American Type Culture Collection (CRL-1772TM). Cells were treated with NR (1 mM) with or without EX527 (10 μM; E7034, Sigma-Aldrich). C2C12 myoblasts were cultured in Dulbecco's modified Eagle's medium (DMEM), including glucose (4.5 g/liter), 10% fetal calf serum, and gentamicin (50 μg/ml). Differentiation of C2C12 cells into myotubes was induced for more

than 4 days in DMEM, including glucose (4.5 g/liter), 2% horse serum, and gentamicin (50 μg/ml). Cells were tested for mycoplasma using MycoProbe (#CUL001B, R&D Systems), following the manufacturer's instructions.

Creatine kinase

Collected plasma was used for creatine kinase measurements using the Creatine Kinase Flex Reagent Cartridge (Siemens Healthcare Diagnostics AG) on the Dimension Xpand Plus Instrument (Siemens Healthcare Diagnostics AG).

Histology

Histological specimens were prepared and analyzed as previously described (17). Muscle damage was assessed with 1% solution of Evans Blue dye (EBD), which is injected into the peritoneal cavity, using 1% volume to body weight, 24 hours before sacrifice. EBD is dissolved in phosphate-buffered saline (PBS) [0.15 M NaCl, 10 mM phosphate buffer (pH 7.4)] and sterilized by passage through membrane filters with a 0.2-μm pore size. Upon sacrifice, the hind leg skin of the mice is removed, and the animals are photographed for dye uptake into skeletal muscles, indicated by blue coloration. Muscle sections from EBD-injected animals are incubated in ice-cold acetone at −20°C for 10 min, washed three times for 10 min with PBS, counter-stained with DAPI and mounted with VECTASHIELD Mounting Medium. Microscopy images of red emission fluorescence from EBD-positive muscle fibers were analyzed using ImageJ software.

We determined the minimal Feret's diameter and cross-sectional area in tibialis anterior muscles of chow diet– and NR-fed *mdx* mice using the ImageJ software quantification of laminin-stained muscle images. We analyzed a minimum of 3000 fibers for each condition and measurement. The minimal Feret's diameter is defined as the minimum distance between two parallel tangents at opposing borders of the muscle fiber. This measure has been found to be resistant to deviations away from the optimal cross-sectioning profile during the sectioning process (48).

Enzyme activity measurements

Total PARP activity was analyzed in tissue homogenates using the HT Colorimetric PARP Apoptosis Assay Kit (Trevigen). This PARP activity assay kit is sensitive to PARylation of proteins that are 2 U of PAR in length and larger. CS activity was determined in tissue homogenates using a commercial CS assay kit (Sigma).

Tissue and C2C12 cell NAD^+ quantification

NAD^+ was extracted using acidic extraction method and analyzed with mass spectrometry. Frozen muscle tissues or cultured cells taken from the −80°C freezer were immediately extracted in 1 M perchloric acid and neutralized in 3 M K_2CO_3 on ice. After centrifugation, the supernatant was mixed with buffer A [H_2O + 20 mM ammonium acetate (pH 9.4)] and loaded onto a column (150 × 2.1 mm; Kinetex EVO C18, 100 Å). HPLC was run for 2 min at a flow rate of 300 ml/min with 100% buffer A. Then, a linear gradient to 100% buffer B [methanol + 5 mM ammonium acetate (pH 8.5)] was performed (at 2 to 11 min). Buffer B (100%) was maintained for 4 min (at 11 to 15 min), and then a linear gradient back to 100%

buffer A (at 15 to 17 min) began. Buffer A was then maintained at 100% until the end (at 17 to 25 min). NAD^+ eluted as a sharp peak at 3.3 min and was quantified on the basis of the peak area compared to a standard curve and normalized to tissue weight or protein of frozen muscle tissues or to the protein content of cultured cells.

Identification of *Nampt*- and *Parp1*-correlated genes and parameters

Quadriceps microarray data (Affymetrix Mouse Gene 1.0 ST) and phenotyping data from a BXD mouse genetic reference population (20) were analyzed for correlations with *Nampt* or *Parp1* transcript expression using the GeneNetwork program. All raw data are publicly available on National Center for Biotechnology Information Gene Expression Omnibus (GSE60151) and on GeneNetwork (www.genenetwork.org).

Gene expression analyses

Total muscle RNA extracted using TRIzol was transcribed to complementary DNA using QuantiTect Reverse Transcription Kit (Qiagen). Expression of selected genes was analyzed using the LightCycler 480 System (Roche) and SYBR Green chemistry. All quantitative polymerase chain reaction (PCR) results were presented relative to the mean of *36b4, B2m*, and *Gapdh* ($\Delta\Delta C_t$ method). Primer sets for quantitative reverse transcription PCR (qRT-PCR) analyses are shown in table S1.

Western blotting and blue native PAGE

Samples were lysed in lysis buffer [50 mM tris (pH 7.4), 150 mM KCl, 1 mM EDTA, 1% NP-40, 5 mM NAM, 1 mM sodium butyrate, protease inhibitors]. Proteins were separated by SDS-PAGE and transferred onto nitrocellulose or polyvinylidene difluoride membranes. Blocking and antibody incubations were performed in 5% bovine serum albumin. SIRT1 antibody was from Abcam, anti-FOXO1 antibody was from Cell Signaling, PAR antibody was from Millipore, and anti–acetyl-FRKH (FOXO) antibody was from Santa Cruz Biotechnology. Antibody cocktail (the MitoProfile Total OXPHOS Rodent WB Antibody Cocktail) for mitochondrial subunits was purchased from MitoSciences. Antibody detection reactions were developed by enhanced chemiluminescence (Advansta) using x-ray films or imaged using the c300 imaging system (Azure Biosystems). Quantification was done using ImageJ software. Blue native PAGE on isolated mitochondria from muscle or C2C12 cells was performed using the NativePAGE Novex Bis-Tris Gel System (Invitrogen), as described previously (49).

Respirometry on C2C12 myotubes

C2C12 myotubes in suspension were used to measure basal respiration rates using high-resolution respirometry (Oxygraph-2k, OROBOROS Instruments), as described previously (50). Then, oligomycin (2.5 μM), a complex V inhibitor, was injected to measure proton leak, and then the protonophore agent FCCP (0.2 mM) was titrated to achieve maximum electron transfer flux. O_2 flux obtained in each step of the protocol was normalized by the protein content of the sample used for the analysis.

In vivo spectroscopy and data analysis

A Bruker 14-T magnet was used to study the mouse hindlimb muscle (51). Briefly, mice were fasted overnight and then given food ad libitum 2 hours before performing MRS and optical spectroscopy. Mice were anesthetized using 2.5% tribromoethanol (0.01 ml/g). Left distal hindlimbs are shaved and cleared of dander, and mice are situated in place using flexible hook and loop-fastening straps to the inside of a custom-built MR/optics probe for the vertical bore 14-T spectrometer (Bruker), as previously described (51). Shaved distal hindlimbs were centered inside a horizontal MR solenoid coil with fiber optic wires situation to either side of the hindlimb. The MR solenoid coil was tuned and matched to ^{1}H and ^{31}P, and MR was optimized by shimming the ^{1}H signal of tissue H_2O. ^{31}P spectra were then acquired using fully relaxed conditions with proton decoupling (80 transients, 4096 complex points, 20-kHz sweep width, and 30-s interpulse delay). Dynamic MR (45° flip angle, 4 transients, 4096 complex points, 20-kHz sweep width, and 1.5-s interpulse delay) was acquired in the following periods: rest (2 min), ischemia (9 min), and recovery (9 min). O_2 (100%) was administered starting after 1 min of rest during the dynamic phase and continued throughout the experiment. All fully relaxed spectra were Fourier-transformed with apodization of 40 Hz and baseline-corrected. Detailed conditions and analysis of MRS data for ATP fluxes and NAD^+ are found in the Supplementary Materials.

In vivo measurement of isometric torque and induction of muscle injury

These experiments were performed as described (52). Briefly, animals were anesthetized using ~2% isoflurane inhalation, and sterile ophthalmic cream was applied on each eye. Under a heat lamp, a needle (25 gauge) was manually placed through the distal femur to stabilize the femur onto the rig. The ankle was then secured to a custom-machined adjustable lever arm with adhesive tape. The ankle rod was adjusted so that it lies anteriorly on the distal leg just above the foot. The position of the ankle rod was not altered between age-matched animals of the same species so that the lever would be constant between tests. The lever arm was attached to a stepper motor (model T8904, NMB Technologies) and a torque sensor (model QWFK-8M, Sensotec). Subcutaneous electrodes (J05 Needle Electrode Needles, 36BTP, Jari Electrode Supply) were used to stimulate the femoral nerve. To obtain maximal isometric torque, the pulse amplitude was adjusted to optimize twitch tension, and the optimal position of the leg was determined by measuring twitches at different lengths of the quadriceps. Using a commercial software (LabVIEW version 2013, National Instruments), each experiment synchronizes contractile activation, the onset of knee rotation, and torque data collection. To assess injury during force lengthening contractions, stimulation of the quadriceps muscles was performed, whereas a computer-controlled motor simultaneously moved the lever arm against the direction of knee extension. This led to a lengthening (eccentric) contraction. The loss of force production during maximal and repeated lengthening contractions was a result of muscle injury. A maximal tetanic contraction is then obtained to determine maximal contractile tension (P_0). Maximal tetanic contractions can be performed repeatedly over time, with the final tension expressed as percentage of P_0.

C. elegans studies

C. elegans movement was recorded for 45 s at days 1 to 8 of adulthood using a Nikon DS-L2/DS-Fi1 camera and controller setup, attached to both a computer and a standard bright-field microscope. The movement of worms during aging was calculated by following worm centroids using a modified version of the freely available software Parallel Worm Tracker for MATLAB (10). These experiments were repeated at least three times.

Treatments were performed by adding NR (1 mM) or mNAM (1 mM or 1 μM; Sigma) dissolved in water and added into nematode growth medium (NGM) agar just before pouring the plates. Worms were exposed to NR during the full life, from eggs until death. To ensure a permanent exposure to the compound, plates were changed twice a week. Worm paralysis was assessed as previously described (53). Experiments with heat-inactivated bacteria were performed by placing OP50 *Escherichia coli* into a water bath at 65°C for 35 min.

Muscle degeneration experiments were performed on 90-mm petri dishes containing NGM agar. Plates were induced overnight at room temperature with 4 mM isopropyl-β-D-thiogalactopyranoside and seeded with HT115 bacteria expressing either empty vector RNAi L4440 or *sir-2.1* RNAi clone (R11A8.4, clone purchased from Geneservice and sequenced) grown in LB medium with ampicillin (100 μg/ml) and tetracycline (12.5 μg/ml) until reaching an optic density between 0.6 and 0.8. Synchronized egg populations of *dys-1(cx18);hlh-1(cc561ts)* double-mutant animals (31) were cultured at 15°C for 8 days and harvested for a 25-min fixation in 1 ml of PBS supplemented with 20 μl of 37% formaldehyde. Samples were then permeabilized using cold methanol for 2 min and stained by rhodamine-coupled phalloidin, a marker of filamentous actin, as described previously (54). Using a Zeiss Axioplan microscope (objective, ×40), the two most visible muscle quadrants of each animal were scored for missing cells or cells showing fragmented, aggregated, or destroyed actin fibers (40 cells per animal and at least 60 worms per condition were examined per experiment). All experiments were performed blindly three times and compared using Student's *t* test. Illustrative images of the actin network for each condition were recorded using a Zeiss LSM 510 meta fluorescence confocal microscope (objective, ×40) and analyzed using Image J.

Statistics

Differences between two groups were assessed using two-tailed *t* tests. Differences between more than two groups were assessed using one-way analysis of variance (ANOVA). To compare the interaction between two factors, two-way ANOVA tests were performed. ANOVA, assessed by Bonferroni's multiple-comparison test, was used when comparing more than two groups. GraphPad Prism 5 was used for all statistical analyses. All P values <0.05 were considered significant. *$P \leq 0.05$, **$P \leq 0.01$, and ***$P \leq 0.001$.

Supplementary Material

Refer to Web version on PubMed Central for supplementary material.

Acknowledgments

We thank T. Vogt for enhancing scientific connectivity and Y. Terrada for scientific discussions. We also thank J. Lunde for his technical expertise with mouse models of muscular dystrophy. **Funding**: K.J.M. is supported by the University of Ottawa and an Interdisciplinary School of Health Sciences Accelerator Initiative award and was the recipient of a Heart and Stroke Foundation of Canada research fellowship award. J.A. is the Nestlé Chair in Energy Metabolism, and his research is supported by the École Polytechnique Fédérale de Lausanne (EPFL), NIH (R01AG043930), the Krebsforschung Schweiz/ Swiss Cancer League (KFS-3082-02-2013), Systems X (SySX.ch 2013/153), and the Swiss National Science Foundation (310030B-160318). H.Z. is a recipient of a doctoral scholarship from the China Scholarship Council and a fellowship from CARIGEST SA. V.S. is supported by the "EPFL Fellows" program co-funded by the Marie Skłodowska-Curie, Horizon 2020 Grant (665667). S.B. and L.W. are supported by the FRM (Fondation pour la Recherche Medicale). C.C. is an employee of the Nestlé Institute of Health Sciences.

REFERENCES AND NOTES

1. Moat SJ, Bradley DM, Salmon R, Clarke A, Hartley L. Newborn bloodspot screening for Duchenne muscular dystrophy: 21 years experience in Wales (UK). Eur. J. Hum. Genet. 2013; 21:1049–1053. [PubMed: 23340516]
2. Mendell JR, Shilling C, Leslie ND, Flanigan KM, al-Dahhak R, Gastier-Foster J, Kneile K, Dunn DM, Duval B, Aoyagi A, Hamil C, Mahmoud M, Roush K, Bird L, Rankin C, Lilly H, Street N, Chandrasekar R, Weiss RB. Evidence-based path to newborn screening for Duchenne muscular dystrophy. Ann. Neurol. 2012; 71:304–313. [PubMed: 22451200]
3. Fairclough RJ, Wood MJ, Davies KE. Therapy for Duchenne muscular dystrophy: Renewed optimism from genetic approaches. Nat. Rev. Genet. 2013; 14:373–378. [PubMed: 23609411]
4. Chalkiadaki A, Igarashi M, Nasamu AS, Knezevic J, Guarente L. Muscle-specific SIRT1 gain-of-function increases slow-twitch fibers and ameliorates pathophysiology in a mouse model of Duchenne muscular dystrophy. PLOS Genet. 2014; 10:e1004490. [PubMed: 25032964]
5. Handschin C, Kobayashi YM, Chin S, Seale P, Campbell KP, Spiegelman BM. PGC-1α regulates the neuromuscular junction program and ameliorates Duchenne muscular dystrophy. Genes Dev. 2007; 21:770–783. [PubMed: 17403779]
6. Sandri M, Lin J, Handschin C, Yang W, Arany ZP, Lecker SH, Goldberg AL, Spiegelman BM. PGC-1α protects skeletal muscle from atrophy by suppressing FoxO3 action and atrophy-specific gene transcription. Proc. Natl. Acad. Sci. U.S.A. 2006; 103:16260–16265. [PubMed: 17053067]
7. Lee D, Goldberg AL. SIRT1 protein, by blocking the activities of transcription factors FoxO1 and FoxO3, inhibits muscle atrophy and promotes muscle growth. J. Biol. Chem. 2013; 288:30515–30526. [PubMed: 24003218]
8. Bonaldo P, Sandri M. Cellular and molecular mechanisms of muscle atrophy. Dis. Models & Mech. 2013; 6:25–39.
9. Cantó C, Houtkooper RH, Pirinen E, Youn DY, Oosterveer MH, Cen Y, Fernandez-Marcos PJ, Yamamoto H, Andreux PA, Cettour-Rose P, Gademann K, Rinsch C, Schoonjans K, Sauve AA, Auwerx J. The NAD^+ precursor nicotinamide riboside enhances oxidative metabolism and protects against high-fat diet-induced obesity. Cell Metab. 2012; 15:838–847. [PubMed: 22682224]
10. Mouchiroud L, Houtkooper RH, Moullan N, Katsyuba E, Ryu D, Cantó C, Mottis A, Jo Y-S, Viswanathan M, Schoonjans K, Guarente L, Auwerx J. The NAD^+/sirtuin pathway modulates longevity through activation of mitochondrial UPR and FOXO signaling. Cell. 2013; 154:430–441. [PubMed: 23870130]
11. Pirinen E, Cantó C, Jo YS, Morato L, Zhang H, Menzies KJ, Williams EG, Mouchiroud L, Moullan N, Hagberg C, Li W, Timmers S, Imhof R, Verbeek J, Pujol A, van Loon B, Viscomi C, Zeviani M, Schrauwen P, Sauve AA, Schoonjans K, Auwerx J. Pharmacological Inhibition of poly(ADP-ribose) polymerases improves fitness and mitochondrial function in skeletal muscle. Cell Metab. 2014; 19:1034–1041. [PubMed: 24814482]
12. Yoshino J, Mills KF, Yoon MJ, Imai S-i. Nicotinamide mononucleotide, a key NAD^+ intermediate, treats the pathophysiology of diet- and age-induced diabetes in mice. Cell Metab. 2011; 14:528–536. [PubMed: 21982712]

13. Gomes AP, Price NL, Ling AJY, Moslehi JJ, Montgomery MK, Rajman L, White JP, Teodoro JS, Wrann CD, Hubbard BP, Mercken EM, Palmeira CM, de Cabo R, Rolo AP, Turner N, Bell EL, Sinclair DA. Declining NAD^+ induces a pseudohypoxic state disrupting nuclear-mitochondrial communication during aging. Cell. 2013; 155:1624–1638. [PubMed: 24360282]
14. Gariani K, Menzies KJ, Ryu D, Wegner CJ, Wang X, Ropelle ER, Moullan N, Zhang H, Perino A, Lemos V, Kim B, Park Y-K, Piersigilli A, Pham TX, Yang Y, Ku CS, Koo SI, Fomitchova A, Cantó C, Schoonjans K, Sauve AA, Lee JY, Auwerx J. Eliciting the mitochondrial unfolded protein response by nicotinamide adenine dinucleotide repletion reverses fatty liver disease in mice. Hepatology. 2016; 63:1190–1204. [PubMed: 26404765]
15. Bai P, Cantó C, Oudart H, Brunyánszki A, Cen Y, Thomas C, Yamamoto H, Huber A, Kiss B, Houtkooper RH, Schoonjans K, Schreiber V, Sauve AA, Menissier-de Murcia J, Auwerx J. PARP-1 inhibition increases mitochondrial metabolism through SIRT1 activation. Cell Metab. 2011; 13:461–468. [PubMed: 21459330]
16. Aguennouz MH, Vita GL, Messina S, Cama A, Lanzano N, Ciranni A, Rodolico C, Di Giorgio RM, Vita G. Telomere shortening is associated to TRF1 and PARP1 overexpression in Duchenne muscular dystrophy. Neurobiol. Aging. 2011; 32:2190–2197. [PubMed: 20137830]
17. Zhang H, Ryu D, Wu Y, Gariani K, Wang X, Luan P, D'Amico D, Ropelle ER, Lutolf MP, Aebersold R, Schoonjans K, Menzies KJ, Auwerx J. NAD^+ repletion improves mitochondrial and stem cell function and enhances life span in mice. Science. 2016; 352:1436–1443. [PubMed: 27127236]
18. Goody MF, Kelly MW, Reynolds CJ, Khalil A, Crawford BD, Henry CA. NAD+ biosynthesis ameliorates a zebrafish model of muscular dystrophy. PLOS Biol. 2012; 10:e1001409. [PubMed: 23109907]
19. Cantó C, Menzies KJ, Auwerx J. NAD^+ metabolism and the control of energy homeostasis: A balancing act between mitochondria and the nucleus. Cell Metab. 2015; 22:31–53. [PubMed: 26118927]
20. Andreux PA, Williams EG, Koutnikova H, Houtkooper RH, Champy M-F, Henry H, Schoonjans K, Williams RW, Auwerx J. Systems genetics of metabolism: The use of the BXD murine reference panel for multiscalar integration of traits. Cell. 2012; 150:1287–1299. [PubMed: 22939713]
21. Williams EG, Wu Y, Jha P, Dubuis S, Blattmann P, Argmann CA, Houten SM, Amariuta T, Wolski W, Zamboni N, Aebersold R, Auwerx J. Systems proteomics of liver mitochondria function. Science. 2016; 352:aad0189. [PubMed: 27284200]
22. Wu Y, Williams EG, Dubuis S, Mottis A, Jovaisaite V, Houten SM, Argmann CA, Faridi P, Wolski W, Kutalik Z, Zamboni N, Auwerx J, Aebersold R. Multilayered genetic and omics dissection of mitochondrial activity in a mouse reference population. Cell. 2014; 158:1415–1430. [PubMed: 25215496]
23. Subramanian A, Tamayo P, Mootha VK, Mukherjee S, Ebert BL, Gillette MA, Paulovich A, Pomeroy SL, Golub TR, Lander ES, Mesirov JP. Gene set enrichment analysis: A knowledge-based approach for interpreting genome-wide expression profiles. Proc. Natl. Acad. Sci. U.S.A. 2005; 102:15545–15550. [PubMed: 16199517]
24. Bakay M, Wang Z, Melcon G, Schiltz L, Xuan J, Zhao P, Sartorelli V, Seo J, Pegoraro E, Angelini C, Shneiderman B, Escolar D, Chen Y-W, Winokur ST, Pachman LM, Fan C, Mandler R, Nevo Y, Gordon E, Zhu Y, Dong Y, Wang Y, Hoffman EP. Nuclear envelope dystrophies show a transcriptional fingerprint suggesting disruption of Rb-MyoD pathways in muscle regeneration. Brain. 2006; 129:996–1013. [PubMed: 16478798]
25. Dadgar S, Wang Z, Johnston H, Kesari A, Nagaraju K, Chen Y-W, Hill DA, Partridge TA, Giri M, Freishtat RJ, Nazarian J, Xuan J, Wang Y, Hoffman EP. Asynchronous remodeling is a driver of failed regeneration in Duchenne muscular dystrophy. J. Cell Biol. 2014; 207:139–158. [PubMed: 25313409]
26. Kraus D, Yang Q, Kong D, Banks AS, Zhang L, Rodgers JT, Pirinen E, Pulinilkunnil TC, Gong F, Wang Y-c, Cen Y, Sauve AA, Asara JM, Peroni OD, Monia BP, Bhanot S, Alhonen L, Puigserver P, Kahn BB. Nicotinamide N-methyltransferase knockdown protects against diet-induced obesity. Nature. 2014; 508:258–262. [PubMed: 24717514]

27. Aksoy S, Szumlanski CL, Weinshilboum RM. Human liver nicotinamide N-methyltransferase. cDNA cloning, expression, and biochemical characterization. J. Biol. Chem. 1994; 269:14835–14840. [PubMed: 8182091]
28. Houtkooper RH, Cantó C, Wanders RJ, Auwerx J. The secret life of NAD^+: An old metabolite controlling new metabolic signaling pathways. Endocr. Rev. 2010; 31:194–223. [PubMed: 20007326]
29. Percival JM, Whitehead NP, Adams ME, Adamo CM, Beavo JA, Froehner SC. Sildenafil reduces respiratory muscle weakness and fibrosis in the *mdx* mouse model of Duchenne muscular dystrophy. J. Pathol. 2012; 228:77–87. [PubMed: 22653783]
30. Belenky P, Racette FG, Bogan KL, McClure JM, Smith JS, Brenner C. Nicotinamide riboside promotes Sir2 silencing and extends lifespan via Nrk and Urh1/Pnp1/Meu1 pathways to NAD^+ Cell. 2007; 129:473–484. [PubMed: 17482543]
31. Gieseler K, Grisoni K, Ségalat L. Genetic suppression of phenotypes arising from mutations in dystrophin-related genes in *Caenorhabditis elegans*. Curr. Biol. 2000; 10:1092–1097. [PubMed: 10996789]
32. Schmeisser K, Mansfeld J, Kuhlow D, Weimer S, Priebe S, Heiland I, Birringer M, Groth M, Segref A, Kanfi Y, Price NL, Schmeisser S, Schuster S, Pfeiffer AFH, Guthke R, Platzer M, Hoppe T, Cohen HY, Zarse K, Sinclair DA, Ristow M. Role of sirtuins in lifespan regulation is linked to methylation of nicotinamide. Nat. Chem. Biol. 2013; 9:693–700. [PubMed: 24077178]
33. Quinlan JG, Hahn HS, Wong BL, Lorenz JN, Wenisch AS, Levin LS. Evolution of the mdx mouse cardiomyopathy: Physiological and morphological findings. Neuromuscul Disord. 2004; 14:491–496. [PubMed: 15336690]
34. Yeung F, Hoberg JE, Ramsey CS, Keller MD, Jones DR, Frye RA, Mayo MW. Modulation of NF-κB-dependent transcription and cell survival by the SIRT1 deacetylase. EMBO J. 2004; 23:2369–2380. [PubMed: 15152190]
35. Joe AWB, Yi L, Natarajan A, Le Grand F, So L, Wang J, Rudnicki MA, Rossi FM. Muscle injury activates resident fibro/adipogenic progenitors that facilitate myogenesis. Nat. Cell Biol. 2010; 12:153–163. [PubMed: 20081841]
36. Heredia JE, Mukundan L, Chen FM, Mueller AA, Deo RC, Locksley RM, Rando TA, Chawla A. Type 2 innate signals stimulate fibro/adipogenic progenitors to facilitate muscle regeneration. Cell. 2013; 153:376–388. [PubMed: 23582327]
37. Sciorati C, Clementi E, Manfredi AA, Rovere-Querini P. Fat deposition and accumulation in the damaged and inflamed skeletal muscle: Cellular and molecular players. Cell. Mol. Life Sci. 2015; 72:2135–2156. [PubMed: 25854633]
38. Cordani N, Pisa V, Pozzi L, Sciorati C, Clementi E. Nitric oxide controls fat deposition in dystrophic skeletal muscle by regulating fibro-adipogenic precursor differentiation. Stem Cells. 2014; 32:874–885. [PubMed: 24170326]
39. Mukhopadhyay P, Rajesh M, Cao Z, Horváth B, Park O, Wang H, Erdelyi K, Holovac E, Wang Y, Liaudet L, Hamdaoui N, Lafdil F, Haskó G, Szabo C, Boulares AH, Gao B, Pacher P. Poly (ADP-ribose) polymerase-1 is a key mediator of liver inflammation and fibrosis. Hepatology. 2014; 59:1998–2009. [PubMed: 24089324]
40. van de Weijer T, Phielix E, Bilet L, Williams EG, Ropelle ER, Bierwagen A, Livingstone R, Nowotny P, Sparks LM, Paglialunga S, Szendroedi J, Havekes B, Moullan N, Pirinen E, Hwang J-H, Schrauwen-Hinderling VB, Hesselink MKC, Auwerx J, Roden M, Schrauwen P. Evidence for a direct effect of the NAD^+ precursor Acipimox on muscle mitochondrial function in humans. Diabetes. 2014; 64:1193–1201. [PubMed: 25352640]
41. Van Gool F, Gallí M, Gueydan C, Kruys V, Prevot P-P, Bedalov A, Mostoslavsky R, Alt FW, De Smedt T, Leo O. Intracellular NAD levels regulate tumor necrosis factor protein synthesis in a sirtuin-dependent manner. Nat. Med. 2009; 15:206–210. [PubMed: 19151729]
42. Giansanti V, Donà F, Tillhon M, Scovassi AI. PARP inhibitors: New tools to protect from inflammation. Biochem. Pharmacol. 2010; 80:1869–1877. [PubMed: 20417190]
43. Traba J, Kwarteng-Siaw M, Okoli TC, Li J, Huffstutler RD, Bray A, Waclawiw MA, Han K, Pelletier M, Sauve AA, Siegel RM, Sack MN. Fasting and refeeding differentially regulate NLRP3

inflammasome activation in human subjects. J. Clin. Invest. 2015; 125:4592–4600. [PubMed: 26529255]

44. Brunet A, Sweeney LB, Sturgill JF, Chua KF, Greer PL, Lin Y, Tran H, Ross SE, Mostoslavsky R, Cohen HY, Hu LS, Cheng H-L, Jedrychowski MP, Gygi SP, Sinclair DA, Alt FW, Greenberg ME. Stress-dependent regulation of FOXO transcription factors by the SIRT1 deacetylase. Science. 2004; 303:2011–2015. [PubMed: 14976264]
45. Champy M-F, Selloum M, Zeitler V, Caradec C, Jung B, Rousseau S, Pouilly L, Sorg T, Auwerx J. Genetic background determines metabolic phenotypes in the mouse. Mamm. Genome. 2008; 19:318–331. [PubMed: 18392653]
46. Yamamoto H, Williams EG, Mouchiroud L, Cantó C, Fan W, Downes M, Héligon C, Barish GD, Desvergne B, Evans RM, Schoonjans K, Auwerx J. NCoR1 Is a conserved physiological modulator of muscle mass and oxidative function. Cell. 2011; 147:827–839. [PubMed: 22078881]
47. Lagouge M, Argmann C, Gerhart-Hines Z, Meziane H, Lerin C, Daussin F, Messadeq N, Milne J, Lambert P, Elliott P, Geny B, Laakso M, Puigserver P, Auwerx J. Resveratrol improves mitochondrial function and protects against metabolic disease by activating SIRT1 and PGC-1α. Cell. 2006; 127:1109–1122. [PubMed: 17112576]
48. Cohn RD, van Erp C, Habashi JP, Soleimani AA, Klein EC, Lisi MT, Gamradt M, ap Rhys CM, Holm TM, Loeys BL, Ramirez F, Judge DP, Ward CW, Dietz HC. Angiotensin II type 1 receptor blockade attenuates TGF-β-induced failure of muscle regeneration in multiple myopathic states. Nat. Med. 2007; 13:204–210. [PubMed: 17237794]
49. Ryu D, Jo YS, Lo Sasso G, Stein S, Zhang H, Perino A, Lee JU, Zeviani M, Romand R, Hottiger MO, Schoonjans K, Auwerx J. A SIRT7-dependent acetylation switch of GABPβ1 controls mitochondrial function. Cell Metab. 2014; 20:856–869. [PubMed: 25200183]
50. Moullan N, Mouchiroud L, Wang X, Ryu D, Williams EG, Mottis A, Jovaisaite V, Frochaux MV, Quiros PM, Deplancke B, Houtkooper RH, Auwerx J. Tetracyclines disturb mitochondrial function across eukaryotic models: A call for caution in biomedical research. Cell Rep. 2015; 10:1681–1691.
51. Siegel MP, Wilbur T, Mathis M, Shankland EG, Trieu A, Harper M-E, Marcinek DJ. Impaired adaptability of in vivo mitochondrial energetics to acute oxidative insult in aged skeletal muscle. Mech. Ageing Dev. 2012; 133:620–628. [PubMed: 22935551]
52. Pratt SJP, Lovering RM. A stepwise procedure to test contractility and susceptibility to injury for the rodent quadriceps muscle. J. Biol. Methods. 2014; 1:e8. [PubMed: 25530979]
53. Klionsky DJ, Klionsky DJ, Abdalla FC, Abeliovich H, Abraham RT, Acevedo-Arozena A, Adeli K, Agholme L, Agnello M, Agostinis P, Aguirre-Ghiso JA, Ahn HJ, Ait-Mohamed O, Ait-Si-Ali S, Akematsu T, Akira S, Al-Younes HM, Al-Zeer MA, Albert ML, Albin RL, Alegre-Abarrategui J, Aleo MF, Alirezaei M, Almasan A, Almonte-Becerril M, Amano A, Amaravadi R, Amarnath S, Amer AO, Andrieu-Abadie N, Anantharam V, Ann DK, Anoopkumar-Dukie S, Aoki H, Apostolova N, Arancia G, Aris JP, Asanuma K, Asare NY, Ashida H, Askanas V, Askew DS, Auberger P, Baba M, Backues SK, Baehrecke EH, Bahr BA, Bai XY, Bailly Y, Baiocchi R, Baldini G, Balduini W, Ballabio A, Bamber BA, Bampton ET, Bánhegyi G, Bartholomew CR, Bassham DC, Bast RC Jr, Batoko H, Bay BH, Beau I, Béchet DM, Begley TJ, Behl C, Behrends C, Bekri S, Bellaire B, Bendall LJ, Benetti L, Berliocchi L, Bernardi H, Bernassola F, Besteiro S, Bhatia-Kissova I, Bi X, Biard-Piechaczyk M, Blum JS, Boise LH, Bonaldo P, Boone DL, Bornhauser BC, Bortoluci KR, Bossis I, Bost F, Bourquin JP, Boya P, Boyer-Guittaut M, Bozhkov PV, Brady NR, Brancolini C, Brech A, Brenman JE, Brennand A, Bresnick EH, Brest P, Bridges D, Bristol ML, Brookes PS, Brown EJ, Brumell JH, Brunetti-Pierri N, Brunk UT, Bulman DE, Bultman SJ, Bultynck G, Burbulla LF, Bursch W, Butchar JP, Buzgariu W, Bydlowski SP, Cadwell K, Cahová M, Cai D, Cai J, Cai Q, Calabretta B, Calvo-Garrido J, Camougrand N, Campanella M, Campos-Salinas J, Candi E, Cao L, Caplan AB, Carding SR, Cardoso SM, Carew JS, Carlin CR, Carmignac V, Carneiro LA, Carra S, Caruso RA, Casari G, Casas C, Castino R, Cebollero E, Cecconi F, Celli J, Chaachouay H, Chae HJ, Chai CY, Chan DC, Chan EY, Chang RC, Che CM, Chen CC, Chen GC, Chen GQ, Chen M, Chen Q, Chen SS, Chen W, Chen X, Chen X, Chen X, Chen YG, Chen Y, Chen Y, Chen YJ, Chen Z, Cheng A, Cheng CH, Cheng Y, Cheong H, Cheong JH, Cherry S, Chess-Williams R, Cheung ZH, Chevet E, Chiang HL, Chiarelli R, Chiba T, Chin LS, Chiou SH, Chisari FV, Cho CH, Cho DH, Choi AM, Choi D, Choi KS, Choi ME, Chouaib S, Choubey D, Choubey V, Chu CT, Chuang TH, Chueh SH, Chun T, Chwae YJ, Chye ML, Ciarcia

R, Ciriolo MR, Clague MJ, Clark RS, Clarke PG, Clarke R, Codogno P, Coller HA, Colombo MI, Comincini S, Condello M, Condorelli F, Cookson MR, Coombs GH, Coppens I, Corbalan R, Cossart P, Costelli P, Costes S, Coto-Montes A, Couve E, Coxon FP, Cregg JM, Crespo JL, Cronjé MJ, Cuervo AM, Cullen JJ, Czaja MJ, D'Amelio M, Darfeuille-Michaud A, Davids LM, Davies FE, De Felici M, de Groot JF, de Haan CA, De Martino L, De Milito A, De Tata V, Debnath J, Degterev A, Dehay B, Delbridge LM, Demarchi F, Deng YZ, Dengjel J, Dent P, Denton D, Deretic V, Desai SD, Devenish RJ, Di Gioacchino M, Di Paolo G, Di Pietro C, Díaz-Araya G, Díaz-Laviada I, Diaz-Meco MT, Diaz-Nido J, Dikic I, Dinesh-Kumar SP, Ding WX, Distelhorst CW, Diwan A, Djavaheri-Mergny M, Dokudovskaya S, Dong Z, Dorsey FC, Dosenko V, Dowling JJ, Doxsey S, Dreux M, Drew ME, Duan Q, Duchosal MA, Duff K, Dugail I, Durbeej M, Duszenko M, Edelstein CL, Edinger AL, Egea G, Eichinger L, Eissa NT, Ekmekcioglu S, El-Deiry WS, Elazar Z, Elgendy M, Ellerby LM, Eng KE, Engelbrecht AM, Engelender S, Erenpreisa J, Escalante R, Esclatine A, Eskelinen EL, Espert L, Espina V, Fan H, Fan J, Fan QW, Fan Z, Fang S, Fang Y, Fanto M, Fanzani A, Farkas T, Farré JC, Faure M, Fechheimer M, Feng CG, Feng J, Feng Q, Feng Y, Fésüs L, Feuer R, Figueiredo-Pereira ME, Fimia GM, Fingar DC, Finkbeiner S, Finkel T, Finley KD, Fiorito F, Fisher EA, Fisher PB, Flajolet M, Florez-McClure ML, Florio S, Fon EA, Fornai F, Fortunato F, Fotedar R, Fowler DH, Fox HS, Franco R, Frankel LB, Fransen M, Fuentes JM, Fueyo J, Fujii J, Fujisaki K, Fujita E, Fukuda M, Furukawa RH, Gaestel M, Gailly P, Gajewska M, Galliot B, Galy V, Ganesh S, Ganetzky B, Ganley IG, Gao FB, Gao GF, Gao J, Garcia L, Garcia-Manero G, Garcia-Marcos M, Garmyn M, Gartel AL, Gatti E, Gautel M, Gawriluk TR, Gegg ME, Geng J, Germain M, Gestwicki JE, Gewirtz DA, Ghavami S, Ghosh P, Giammarioli AM, Giatromanolaki AN, Gibson SB, Gilkerson RW, Ginger ML, Ginsberg HN, Golab J, Goligorsky MS, Golstein P, Gomez-Manzano C, Goncu E, Gongora C, Gonzalez CD, Gonzalez R, González-Estévez C, González-Polo RA, Gonzalez-Rey E, Gorbunov NV, Gorski S, Goruppi S, Gottlieb RA, Gozuacik D, Granato GE, Grant GD, Green KN, Gregorc A, Gros F, Grose C, Grunt TW, Gual P, Guan JL, Guan KL, Guichard SM, Gukovskaya AS, Gukovsky I, Gunst J, Gustafsson AB, Halayko AJ, Hale AN, Halonen SK, Hamasaki M, Han F, Han T, Hancock MK, Hansen M, Harada H, Harada M, Hardt SE, Harper JW, Harris AL, Harris J, Harris SD, Hashimoto M, Haspel JA, Hayashi S, Hazelhurst LA, He C, He YW, Hébert MJ, Heidenreich KA, Helfrich MH, Helgason GV, Henske EP, Herman B, Herman PK, Hetz C, Hilfiker S, Hill JA, Hocking LJ, Hofman P, Hofmann TG, Höhfeld J, Holyoake TL, Hong MH, Hood DA, Hotamisligil GS, Houwerzijl EJ, Høyer-Hansen M, Hu B, Hu CA, Hu HM, Hua Y, Huang C, Huang J, Huang S, Huang WP, Huber TB, Huh WK, Hung TH, Hupp TR, Hur GM, Hurley JB, Hussain SN, Hussey PJ, Hwang JJ, Hwang S, Ichihara A, Ilkhanizadeh S, Inoki K, Into T, Iovane V, Iovanna JL, Ip NY, Isaka Y, Ishida H, Isidoro C, Isobe K, Iwasaki A, Izquierdo M, Izumi Y, Jaakkola PM, Jäättelä M, Jackson GR, Jackson WT, Janji B, Jendrach M, Jeon JH, Jeung EB, Jiang H, Jiang H, Jiang JX, Jiang M, Jiang Q, Jiang X, Jiang X, Jiménez A, Jin M, Jin S, Joe CO, Johansen T, Johnson DE, Johnson GV, Jones NL, Joseph B, Joseph SK, Joubert AM, Juhász G, Juillerat-Jeanneret L, Jung CH, Jung YK, Kaarniranta K, Kaasik A, Kabuta T, Kadowaki M, Kagedal K, Kamada Y, Kaminskyy VO, Kampinga HH, Kanamori H, Kang C, Kang KB, Kang KI, Kang R, Kang YA, Kanki T, Kanneganti TD, Kanno H, Kanthasamy AG, Kanthasamy A, Karantza V, Kaushal GP, Kaushik S, Kawazoe Y, Ke PY, Kehrl JH, Kelekar A, Kerkhoff C, Kessel DH, Khalil H, Kiel JA, Kiger AA, Kihara A, Kim DR, Kim DH, Kim DH, Kim EK, Kim HR, Kim JS, Kim JH, Kim JC, Kim JK, Kim PK, Kim SW, Kim YS, Kim Y, Kimchi A, Kimmelman AC, King JS, Kinsella TJ, Kirkin V, Kirshenbaum LA, Kitamoto K, Kitazato K, Klein L, Klimecki WT, Klucken J, Knecht E, Ko BC, Koch JC, Koga H, Koh JY, Koh YH, Koike M, Komatsu M, Kominami E, Kong HJ, Kong WJ, Korolchuk VI, Kotake Y, Koukourakis MI, Kouri Flores JB, Kovács AL, Kraft C, Krainc D, Krämer H, Kretz-Remy C, Krichevsky AM, Kroemer G, Krüger R, Krut O, Ktistakis NT, Kuan CY, Kucharczyk R, Kumar A, Kumar R, Kumar S, Kundu M, Kung HJ, Kurz T, Kwon HJ, La Spada AR, Lafont F, Lamark T, Landry J, Lane JD, Lapaquette P, Laporte JF, László L, Lavandero S, Lavoie JN, Layfield R, Lazo PA, Le W, Le Cam L, Ledbetter DJ, Lee AJ, Lee BW, Lee GM, Lee J, Lee JH, Lee M, Lee MS, Lee SH, Leeuwenburgh C, Legembre P, Legouis R, Lehmann M, Lei HY, Lei QY, Leib DA, Leiro J, Lemasters JJ, Lemoine A, Lesniak MS, Lev D, Levenson VV, Levine B, Levy E, Li F, Li JL, Li L, Li S, Li W, Li XJ, Li YB, Li YP, Liang C, Liang Q, Liao YF, Liberski PP, Lieberman A, Lim HJ, Lim KL, Lim K, Lin CF, Lin FC, Lin J, Lin JD, Lin K, Lin WW, Lin WC, Lin YL, Linden R, Lingor P, Lippincott-Schwartz J, Lisanti MP, Liton PB, Liu B, Liu CF, Liu K, Liu L, Liu QA, Liu W, Liu YC, Liu Y,

Lockshin RA, Lok CN, Lonial S, Loos B, Lopez-Berestein G, López-Otín C, Lossi L, Lotze MT, Lőw P, Lu B, Lu B, Lu B, Lu Z, Luciano F, Lukacs NW, Lund AH, Lynch-Day MA, Ma Y, Macian F, MacKeigan JP, Macleod KF, Madeo F, Maiuri L, Maiuri MC, Malagoli D, Malicdan MC, Malorni W, Man N, Mandelkow EM, Manon S, Manov I, Mao K, Mao X, Mao Z, Marambaud P, Marazziti D, Marcel YL, Marchbank K, Marchetti P, Marciniak SJ, Marcondes M, Mardi M, Marfe G, Mariño G, Markaki M, Marten MR, Martin SJ, Martinand-Mari C, Martinet W, Martinez-Vicente M, Masini M, Matarrese P, Matsuo S, Matteoni R, Mayer A, Mazure NM, McConkey DJ, McConnell MJ, McDermott C, McDonald C, McInerney GM, McKenna SL, McLaughlin B, McLean PJ, McMaster CR, McQuibban GA, Meijer AJ, Meisler MH, Meléndez A, Melia TJ, Melino G, Mena MA, Menendez JA, Menna-Barreto RF, Menon MB, Menzies FM, Mercer CA, Merighi A, Merry DE, Meschini S, Meyer CG, Meyer TF, Miao CY, Miao JY, Michels PA, Michiels C, Mijaljica D, Milojkovic A, Minucci S, Miracco C, Miranti CK, Mitroulis I, Miyazawa K, Mizushima N, Mograbi B, Mohseni S, Molero X, Mollereau B, Mollinedo F, Momoi T, Monastyrska I, Monick MM, Monteiro MJ, Moore MN, Mora R, Moreau K, Moreira PI, Moriyasu Y, Moscat J, Mostowy S, Mottram JC, Motyl T, Moussa CE, Müller S, Muller S, Münger K, Münz C, Murphy LO, Murphy ME, Musarò A, Mysorekar I, Nagata E, Nagata K, Nahimana A, Nair U, Nakagawa T, Nakahira K, Nakano H, Nakatogawa H, Nanjundan M, Naqvi NI, Narendra DP, Narita M, Navarro M, Nawrocki ST, Nazarko TY, Nemchenko A, Netea MG, Neufeld TP, Ney PA, Nezis IP, Nguyen HP, Nie D, Nishino I, Nislow C, Nixon RA, Noda T, Noegel AA, Nogalska A, Noguchi S, Notterpek L, Novak I, Nozaki T, Nukina N, Nürnberger T, Nyfeler B, Obara K, Oberley TD, Oddo S, Ogawa M, Ohashi T, Okamoto K, Oleinick NL, Oliver FJ, Olsen LJ, Olsson S, Opota O, Osborne TF, Ostrander GK, Otsu K, Ou JH, Ouimet M, Overholtzer M, Ozpolat B, Paganetti P, Pagnini U, Pallet N, Palmer GE, Palumbo C, Pan T, Panaretakis T, Pandey UB, Papackova Z, Papassideri I, Paris I, Park J, Park OK, Parys JB, Parzych KR, Patschan S, Patterson C, Pattingre S, Pawelek JM, Peng J, Perlmutter DH, Perrotta I, Perry G, Pervaiz S, Peter M, Peters GJ, Petersen M, Petrovski G, Phang JM, Piacentini M, Pierre P, Pierrefite-Carle V, Pierron G, Pinkas-Kramarski R, Piras A, Piri N, Platanias LC, Pöggeler S, Poirot M, Poletti A, Poüs C, Pozuelo-Rubio M, Prætorius-Ibba M, Prasad A, Prescott M, Priault M, Produit-Zengaffinen N, Progulske-Fox A, Proikas-Cezanne T, Przedborski S, Przyklenk K, Puertollano R, Puyal J, Qian SB, Qin L, Qin ZH, Quaggin SE, Raben N, Rabinowich H, Rabkin SW, Rahman I, Rami A, Ramm G, Randall G, Randow F, Rao VA, Rathmell JC, Ravikumar B, Ray SK, Reed BH, Reed JC, Reggiori F, Régnier-Vigouroux A, Reichert AS, Reiter JJ Jr, Reiners RJ, Ren J, Revuelta JL, Rhodes CJ, Ritis K, Rizzo E, Robbins J, Roberge M, Roca H, Roccheri MC, Rocchi S, Rodemann HP, Rodríguez de Córdoba S, Rohrer B, Roninson IB, Rosen K, Rost-Roszkowska MM, Rouis M, Rouschop KM, Rovetta F, Rubin BP, Rubinsztein DC, Ruckdeschel K, Rucker EB III, Rudich A, Rudolf E, Ruiz-Opazo N, Russo R, Rusten TE, Ryan KM, Ryter SW, Sabatini DM, Sadoshima J, Saha T, Saitoh T, Sakagami H, Sakai Y, Salekdeh GH, Salomoni P, Salvaterra PM, Salvesen G, Salvioli R, Sanchez AM, Sánchez-Alcázar JA, Sánchez-Prieto R, Sandri M, Sankar U, Sansanwal P, Santambrogio L, Saran S, Sarkar S, Sarwal M, Sasakawa C, Sasnauskiene A, Sass M, Sato K, Sato M, Schapira AH, Scharl M, Schätzl HM, Scheper W, Schiaffino S, Schneider C, Schneider ME, Schneider-Stock R, Schoenlein PV, Schorderet DF, Schüller C, Schwartz GK, Scorrano L, Sealy L, Seglen PO, Segura-Aguilar J, Seiliez I, Seleverstov O, Sell C, Seo JB, Separovic D, Setaluri V, Setoguchi T, Settembre C, Shacka JJ, Shanmugam M, Shapiro IM, Shaulian E, Shaw RJ, Shelhamer JH, Shen HM, Shen WC, Sheng ZH, Shi Y, Shibuya K, Shidoji Y, Shieh JJ, Shih CM, Shimada Y, Shimizu S, Shintani T, Shirihai OS, Shore GC, Sibirny AA, Sidhu SB, Sikorska B, Silva-Zacarin EC, Simmons A, Simon AK, Simon HU, Simone C, Simonsen A, Sinclair DA, Singh R, Sinha D, Sinicrope FA, Sirko A, Siu PM, Sivridis E, Skop V, Skulachev VP, Slack RS, Smaili SS, Smith DR, Soengas MS, Soldati T, Song X, Sood AK, Soong TW, Sotgia F, Spector SA, Spies CD, Springer W, Srinivasula SM, Stefanis L, Steffan JS, Stendel R, Stenmark H, Stephanou A, Stern ST, Sternberg C, Stork B, Strålfors P, Subauste CS, Sui X, Sulzer D, Sun J, Sun SY, Sun ZJ, Sung JJ, Suzuki K, Suzuki T, Swanson MS, Swanton C, Sweeney ST, Sy LK, Szabadkai G, Tabas I, Taegtmeyer H, Tafani M, Takács-Vellai K, Takano Y, Takegawa K, Takemura G, Takeshita F, Talbot NJ, Tan KS, Tanaka K, Tanaka K, Tang D, Tang D, Tanida I, Tannous BA, Tavernarakis N, Taylor GS, Taylor GA, Taylor JP, Terada LS, Terman A, Tettamanti G, Thevissen K, Thompson CB, Thorburn A, Thumm M, Tian F, Tian Y, Tocchini-Valentini G, Tolkovsky AM, Tomino Y, Tönges L, Tooze SA, Tournier C, Tower J, Towns R, Trajkovic V, Travassos LH, Tsai TF, Tschan MP, Tsubata T, Tsung A, Turk B, Turner LS, Tyagi

SC, Uchiyama Y, Ueno T, Umekawa M, Umemiya-Shirafuji R, Unni VK, Vaccaro MI, Valente EM, Van den Berghe G, van der Klei IJ, van Doorn W, van Dyk LF, van Egmond M, van Grunsven LA, Vandenabeele P, Vandenberghe WP, Vanhorebeek I, Vaquero EC, Velasco G, Vellai T, Vicencio JM, Vierstra RD, Vila M, Vindis C, Viola G, Viscomi MT, Voitsekhovskaja OV, von Haefen C, Votruba M, Wada K, Wade-Martins R, Walker CL, Walsh CM, Walter J, Wan XB, Wang A, Wang C, Wang D, Wang F, Wang F, Wang G, Wang H, Wang HG, Wang HD, Wang J, Wang K, Wang M, Wang RC, Wang X, Wang X, Wang YJ, Wang Y, Wang Z, Wang ZC, Wang Z, Wansink DG, Ward DM, Watada H, Waters SL, Webster P, Wei L, Weihl CC, Weiss WA, Welford SM, Wen LP, Whitehouse CA, Whitton JL, Whitworth AJ, Wileman T, Wiley JW, Wilkinson S, Willbold D, Williams RL, Williamson PR, Wouters BG, Wu C, Wu DC, Wu WK, Wyttenbach A, Xavier RJ, Xi Z, Xia P, Xiao G, Xie Z, Xie Z, Xu DZ, Xu J, Xu L, Xu X, Yamamoto A, Yamamoto A, Yamashina S, Yamashita M, Yan X, Yanagida M, Yang DS, Yang E, Yang JM, Yang SY, Yang W, Yang WY, Yang Z, Yao MC, Yao TP, Yeganeh B, Yen WL, Yin JJ, Yin XM, Yoo OJ, Yoon G, Yoon SY, Yorimitsu T, Yoshikawa Y, Yoshimori T, Yoshimoto K, You HJ, Youle RJ, Younes A, Yu L, Yu L, Yu SW, Yu WH, Yuan ZM, Yue Z, Yun CH, Yuzaki M, Zabirnyk O, Silva-Zacarin E, Zacks D, Zacksenhaus E, Zaffaroni N, Zakeri Z, Zeh HJ III, Zeitlin SO, Zhang H, Zhang HL, Zhang J, Zhang JP, Zhang L, Zhang L, Zhang MY, Zhang XD, Zhao M, Zhao YF, Zhao Y, Zhao ZJ, Zheng X, Zhivotovsky B, Zhong Q, Zhou CZ, Zhu C, Zhu WG, Zhu XF, Zhu X, Zhu Y, Zoladek T, Zong WX, Zorzano A, Zschocke J, Zuckerbraun B. Guidelines for the use and interpretation of assays for monitoring autophagy. Autophagy. 2012; 8:445–544. [PubMed: 22966490]

54. Waterston RH, Hirsh D, Lane TR. Dominant mutations affecting muscle structure in *Caenorhabditis elegans* that map near the actin gene cluster. J. Mol. Biol. 1984; 180:473–496. [PubMed: 6527380]
55. Ryu D, Mouchiroud L, Andreux PA, Katsyuba E, Moullan N, Nicolet-Dit-Félix AA, Williams EG, Jha P, Lo Sasso G, Huzard D, Aebischer P, Sandi C, Rinsch C, Auwerx J. Urolithin A induces mitophagy and prolongs lifespan in *C. elegans* and increases muscle function in rodents. Nat. Med. 2016; 22:879–888. [PubMed: 27400265]
56. Kushmerick MJ, Dillon PF, Meyer RA, Brown TR, Krisanda JM, Sweeney HL. ^{31}P NMR spectroscopy, chemical analysis, and free Mg^{2+} of rabbit bladder and uterine smooth muscle. J. Biol. Chem. 1986; 261:14420–14429. [PubMed: 3771537]
57. Lu M, Zhu X-H, Zhang Y, Chen W. Intracellular redox state revealed by in vivo ^{31}P MRS measurement of NAD^+ and NADH contents in brains. Magn. Reson. Med. 2014; 71:1959–1972. [PubMed: 23843330]
58. Wiseman RW, Moerland TS, Chase PB, Stuppard R, Kushmerick MJ. High-performance liquid chromatographic assays for free and phosphorylated derivatives of the creatine analogues β-guanidopropionic acid and 1-carboxy-methyl-2-iminoimidazolidine (cyclocreatine). Anal. Biochem. 1992; 204:383–389. [PubMed: 1443539]
59. Heineman FW, Eng J, Berkowitz BA, Balaban RS. NMR spectral analysis of kinetic data using natural lineshapes. Magn. Reson. Med. 1990; 13:490–497. [PubMed: 2325549]
60. Taylor DJ, Bore PJ, Styles P, Gadian DG, Radda GK. Bioenergetics of intact human muscle a ^{31}P Nuclear Resonance Study. Mol. Biol. Med. 1983; 1:77–94. [PubMed: 6679873]

Making muscle work better

Degenerating muscle—whether from muscular dystrophies, myopathies, or other diseases—loses its mitochondria (the energy supply) and an essential cofactor nicotinamide adenine dinucleotide (NAD^+), while gaining an extra load of enzymes that use up NAD^+, as reported by Ryu and colleagues. The resulting loss of NAD^+ is exacerbated by a drop in NAD^+ biosynthetic enzymes, such as NAMPT. Restoration of NAD^+ levels in either mice or worms with disease-like degenerating muscles improved muscle function, a consequence of more mitochondria, more muscle structural proteins, and a decrease in inflammation. The authors suggest that NAD^+ repletion may be a successful therapeutic approach for a number of muscle-wasting diseases.

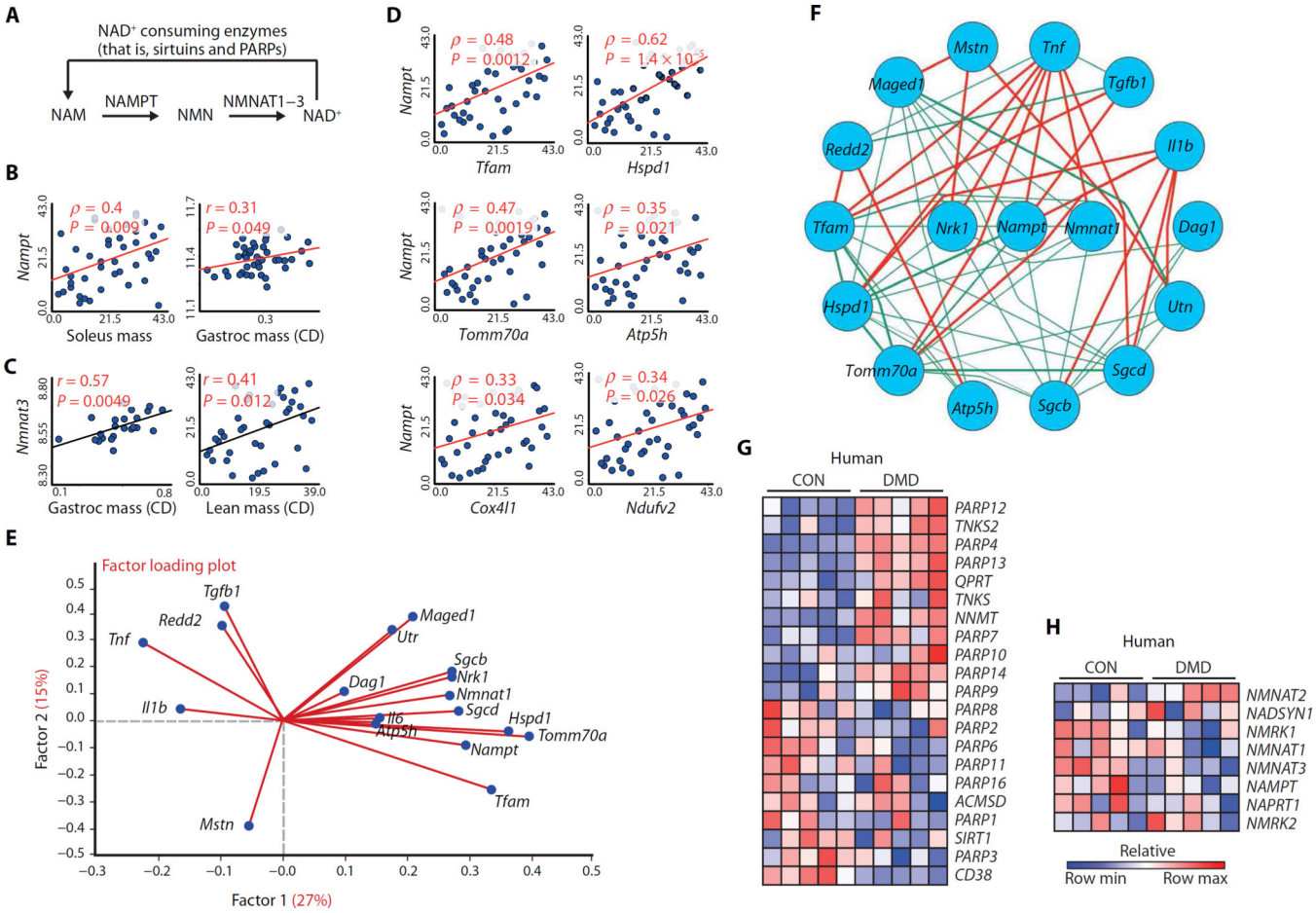

Fig. 1. The relationship between transcripts involved in NAD$^+$ biosynthesis and consumption with muscular dystrophy in mice and DMD patients

(**A**) Schematic illustrating NAD$^+$ consumption by sirtuins and PARPs and the salvage of NAD$^+$ from NAM via NAMPT and NMNAT enzymes. (**B** and **C**) Correlation of *Nampt* (B) and *Nmnat3* (C) transcripts from 42 strains of genetically diverse BXD mice with various measurements of muscle mass, as a percentage of body weight. CD, chow diet. (**D**) Correlation of *Nampt* transcript expression in the BXD strains with transcript expression for regulators of mitochondrial transcription and for genes encoding the components of the mitochondria. (**E**) A factor loading plot (biplot) showing the correlation of transcripts for mitochondrial-related genes (*Tfam, Hspd1, Atp5h*, and *Tomm70a*), utrophin (*Utr*), dystrophin-associated glycoproteins (*Dag1, Sgcb*, and *Sgcd*), muscle growth–related genes (*Maged1* and *Il6*), and genes involved in the pathology of *mdx* mice (*Tgfb1, Tnf, Mstn, Il1b*, and *Redd2*) with NAD$^+$ synthesis transcripts (*Nampt, Nmnat1*, and *Nrk1*) in the BXD mouse strains. Angles more than 90° between gene vectors represent negative correlation (an angle of 180° indicates perfect negative correlation). (**F**) These transcripts were then plotted in a circular schematic using Pearson's $r \geq |0.2|$ in BXD strains showing negative (red) and positive (green) correlations. The expression of transcripts related to NAD$^+$ (**G**) consumption or (**H**) biosynthesis shows an enrichment signature of *PARP* genes and of the *NNMT* gene in human DMD skeletal muscle data sets ($n = 5$ per group) (24, 25). CON, control.

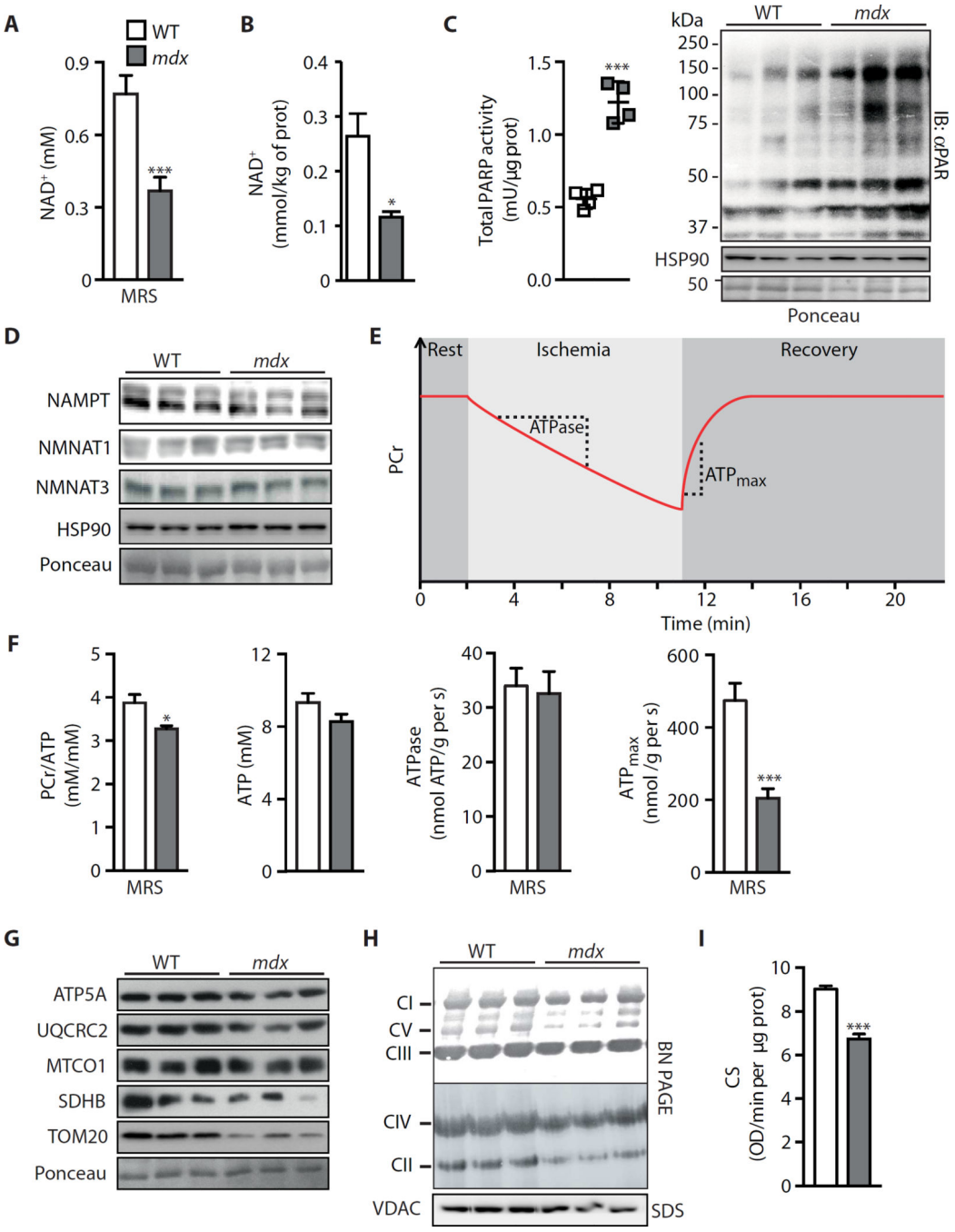

Fig. 2. NAD$^+$ as a marker and limiting factor for in vivo energetics and mitochondrial function in *mdx* mice

Measurements on gastrocnemius from 16-week-old male *mdx* or control mice. As a new marker for muscular dystrophy, (**A**) NAD$^+$ levels were reduced, as measured by ^{31}P MRS [wild type (WT), $n = 7$; *mdx*, $n = 12$]. (**B**) These values paralleled total intracellular NAD$^+$ levels measured by mass spectrometry in tissue extracts ($n = 5$). Reductions in NAD$^+$ levels may be due to augmented NAD$^+$ consumption, evidenced by enhanced (**C**) PARP activity ($n = 4$) and total PARylation content (WT, 1.00 ± 0.25; *mdx*, 2.19 ± 0.31; $P = 0.042$), in

addition to reduced NAD^+ salvage demonstrated by lower (**D**) NAMPT protein (WT, 1.00 ± 0.03; *mdx*, 0.69 ± 0.09; $P = 0.036$), with NMNAT1 (WT, 1.00 ± 0.09; *mdx*, 0.88 ± 0.03) and NMNAT3 (WT, 1.00 ± 0.05; *mdx*, 0.89±0.01; $P = 0.009$) unchanged, using heat shock protein 90 (HSP90) or Ponceau staining as loading controls. prot, protein; IB, immunoblot. (**E**) Schematic of in vivo ^{31}P MRS of *mdx* skeletal muscle mitochondrial energetics. Dynamic magnetic resonance (MR) spectra were acquired during the following periods: rest (2 min), ischemia (9 min), and recovery (9 min). (**F**) High-performance liquid chromatography (HPLC) and ^{31}P MRS measurements of ATP and PCr, respectively, showing unchanged ATP levels ($n = 7$) and a reduction in the PCr/ATP ratio (WT, $n = 7$; *mdx,* $n = 5$). Because the resting ATPase activity did not change (indicating unaltered ATP demand) (WT, $n = 7$; *mdx,* $n = 5$), *mdx* animals must function at an increased fraction of their now reduced maximal capacity (ATP_{max}) (WT, $n = 7$; *mdx,* $n = 5$) to meet the unchanged ATP demand, when MRS data are compared to control animals. *mdx* muscle exhibited corresponding reductions in mitochondrial proteins and function in *mdx* muscle, as represented by (**G**) ATP5A (WT, 1.00 ± 0.06; *mdx*, 0.51 ± 0.04; $P = 0.002$), UQCRC2 (WT, 1.00 ± 0.06; *mdx*, 0.36 ± 0.09; $P = 0.004$), MTCO1 (WT, 1.00 ± 0.20; *mdx*, 0.59 ± 0.04), SDHB (WT, 1.00 ± 0.27; *mdx*, 0.36 ± 0.16), and TOM20 (WT, 1.00 ± 0.07; *mdx*, 0.35 ± 0.12; $P = 0.012$) compared to HSP90 (D) as loading control, (**H**) blue native polyacrylamide gel electrophoresis (BN PAGE) of isolated mitochondria, and (**I**) CS activity ($n = 9$). VDAC, voltage-dependent anion channel; OD, optical density.

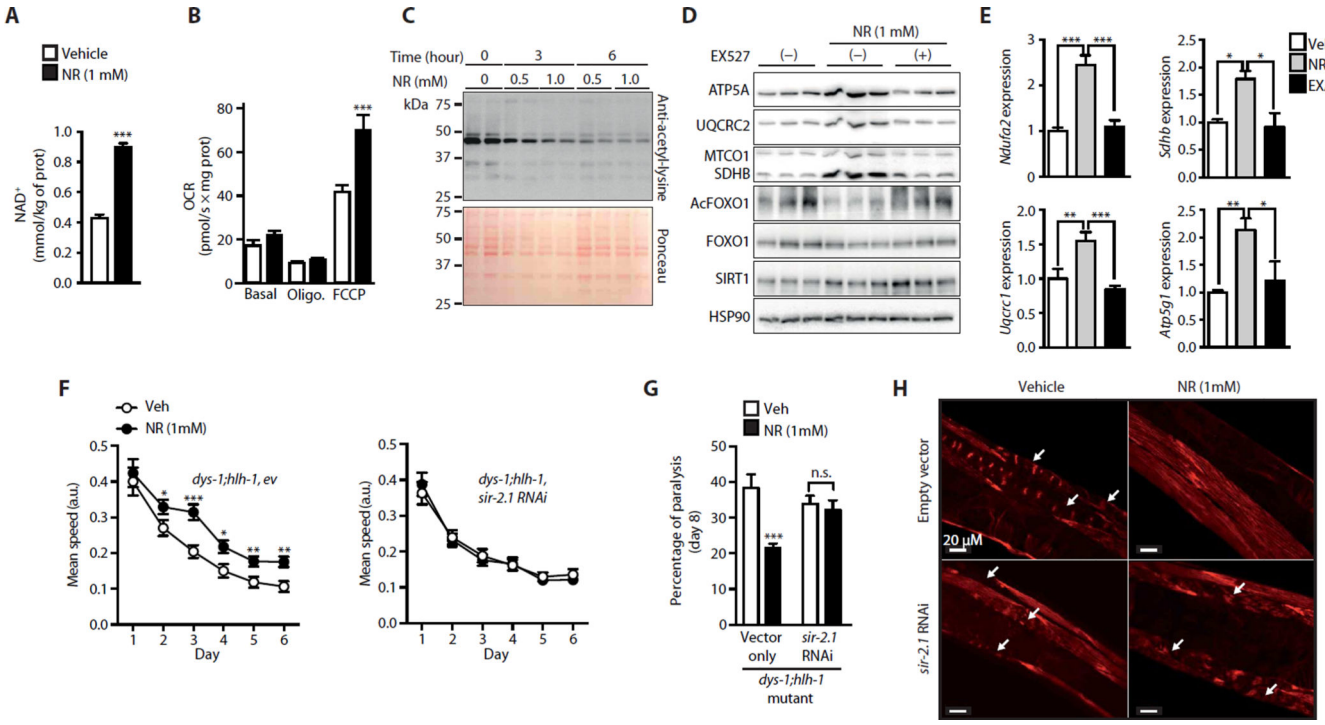

Fig. 3. NR enhances mitochondrial function in C2C12 myotubes and increases SIRT1-dependent muscle integrity and function in *dys-1;hlh-1* double-mutant *C. elegans*

C2C12 myotubes were treated with 0.5 to 1 mM NR. Twelve hours of NR increases (**A**) intracellular NAD^+ levels ($n = 6$) and (**B**) increased oxygen consumption rate (OCR) in myotubes exposed to the uncoupler FCCP ($n = 6$). Veh, vehicle. (**C**) Total protein acetyl-lysine levels in myotubes were reduced after 6 hours of exposure to 0.5 and 1 mM NR. (**D**) SIRT1 inhibition with EX527 (10 μM) in myotubes attenuated increases in mitochondrial proteins [ATP5A (Ctrl, 1.00 ± 0.08; NR, 2.28 ± 0.14; NR + EX527, 0.80 ± 0.24; Ctrl versus NR, $P = 0.001$; NR versus NR + EX527, $P = 0.006$), UQCRC2 (Ctrl, 1.00 ± 0.15; NR, 3.54 ± 0.44; NR + EX527, 1.04 ± 0.17; Ctrl versus NR, $P = 0.006$; NR versus NR + EX527, $P = 0.006$), MTCO1 (Ctrl, 1.00 ± 0.18; NR, 2.25 ± 0.61; NR + EX527, 1.04 ± 0.07), and SDHB (Ctrl, 1.00 ± 0.19; NR, 3.54 ± 0.15; NR + EX527, 1.84 ± 0.11; Ctrl versus NR, $P = 0.001$; NR versus NR + EX527, $P = 0.001$)], reductions in FOXO1 acetylation (Ctrl, 1.00 ± 0.14; NR, 0.46 ± 0.26; NR + EX527, 1.50 ± 0.25; NR versus NR + EX527, $P = 0.044$), and (**E**) inductions of mitochondrial-related transcripts after 12 and 6 hours of NR treatment, respectively. EX, EX527. (**F**) Improvements in *dys-1;hlh-1* mutant worm fitness on days 1 to 6 of adulthood after NR and its *sir-2.1* dependence shown in animals fed RNA interference (RNAi) for *sir-2.1* (R11A8.4), as measured by examining worm motility using the worm tracker ($n = 3$ or 60 worms per experiment) (10). a.u., arbitrary units. Reduced worm paralysis ($n = 3$ or 60 worms per experiment) (**G**) and muscle degeneration, measured by rhodamine-coupled phalloidin staining ($n = 6$ or 60 worms per experiment) (**H**) in *dys-1;hlh-1* mutant worms after NR, were not observed in *dys-1;hlh-1* worms fed RNAi for *sir-2.1*. Arrows indicate degenerated muscle fibers.

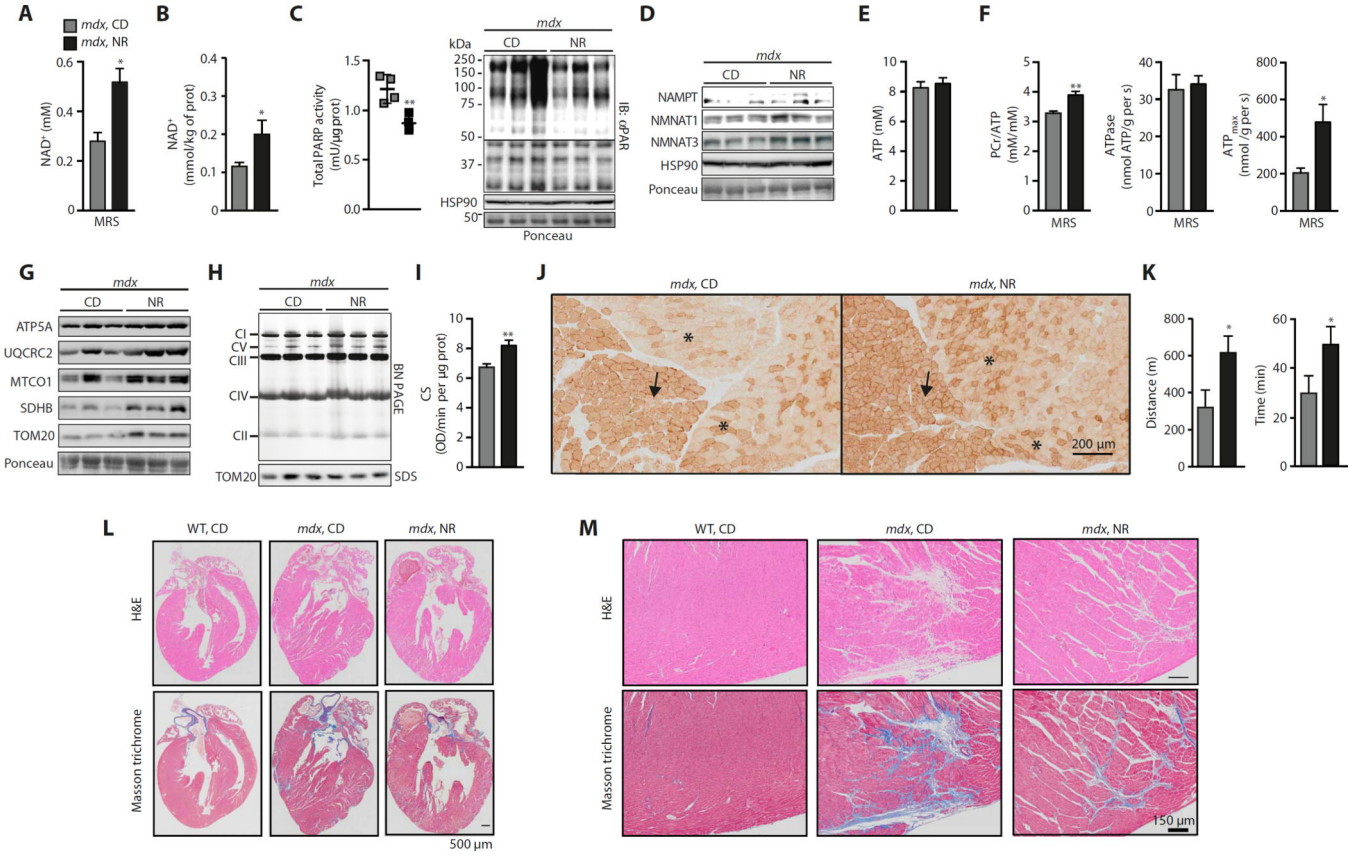

Fig. 4. In vivo monitoring of NAD^+ provides an efficacy marker for improvements in the phenotype of NR-treated *mdx* mice

Sixteen-week-old *mdx* mice received a dietary supplement with NR (400 mg/kg per day) for 12 weeks. (**A**) ^{31}P MRS measurements of increasing NAD^+ levels upon NR treatment in *mdx* mice (*mdx, n* = 5; *mdx* NR, *n* = 10). (**B**) The recovery of *mdx* muscle NAD^+ levels was verified by the analysis of gastrocnemius extracts by mass spectrometry (*n* = 5). (**C**) PARP activity (*n* = 4) and total protein PARylation was reduced (CD, 1.00 ± 0.31; NR, 0.23 ± 0.07; *P* = 0.035), whereas (**D**) NAMPT (CD, 1.00 ± 0.06; NR, 1.20 ± 0.23) and NMNAT3 (CD, 1.00 ± 0.23; NR, 2.64 ± 0.30; *P* = 0.012) content increased, after NR treatment of *mdx* mice. (**E**) Unchanged ATP levels were measured by HPLC in gastrocnemius (*mdx, n* = 7; *mdx* NR, *n* = 10). (**F**) In vivo ^{31}P MRS measurements of mitochondrial energetics revealed an improvement in the PCr/ATP ratio (*mdx, n* = 5; *mdx* NR, *n* = 10), unchanged resting ATPase activity (*mdx, n* = 5; *mdx* NR, *n* = 10), and a recovery of ATP_{max} (*mdx, n* = 5; *mdx* NR, *n* = 10) in NR-treated *mdx* mice. NR-treated *mdx* animals hence function at a reduced fraction of their capacity (ATP_{max}) to meet ATP demand. The enhancement of NAD^+ metabolism with NR prevented improved (**G**) ATP5A (CD, 1.00 ± 0.15; NR, 1.18 ± 0.15), UQCRC2 (CD, 1.00 ± 0.24; NR, 2.21 ± 0.57), MTCO1 (CD, 1.00 ± 0.53; NR, 1.62 ± 0.16), SDHB (CD, 1.00 ± 0.38; NR, 2.96 ± 0.57; *P* = 0.023), and TOM20 (CD, 1.00 ± 0.15; NR, 2.63 ± 0.22; *P* = 0.002) protein levels, using HSP90 (D) or Ponceau loading control, (**H**) mitochondrial complexes as evidenced by blue native PAGE of isolated gastrocnemius mitochondria, using a Coomassie loading control, (**I**) CS activity in frozen gastrocnemius extracts (*mdx, n* = 9; *mdx* NR, *n* = 6), and (**J**) cytochrome c oxidase staining of soleus

(arrow) and gastrocnemius (asterisks) muscle fibers. (**K**) NR increased the running distance and time during an endurance treadmill test in *mdx* mice (*mdx, n* = 9; *mdx* NR, *n* = 12). (**L** and **M**) Hematoxylin and eosin (H&E) and Masson's trichrome staining of hearts from control C57BL/10 and *mdx* male mice at 16 months of age with and without NR treatment. Representative images of the (L) whole heart and (M) magnified sections showing necrosis and fibrosis (*n* = 4).

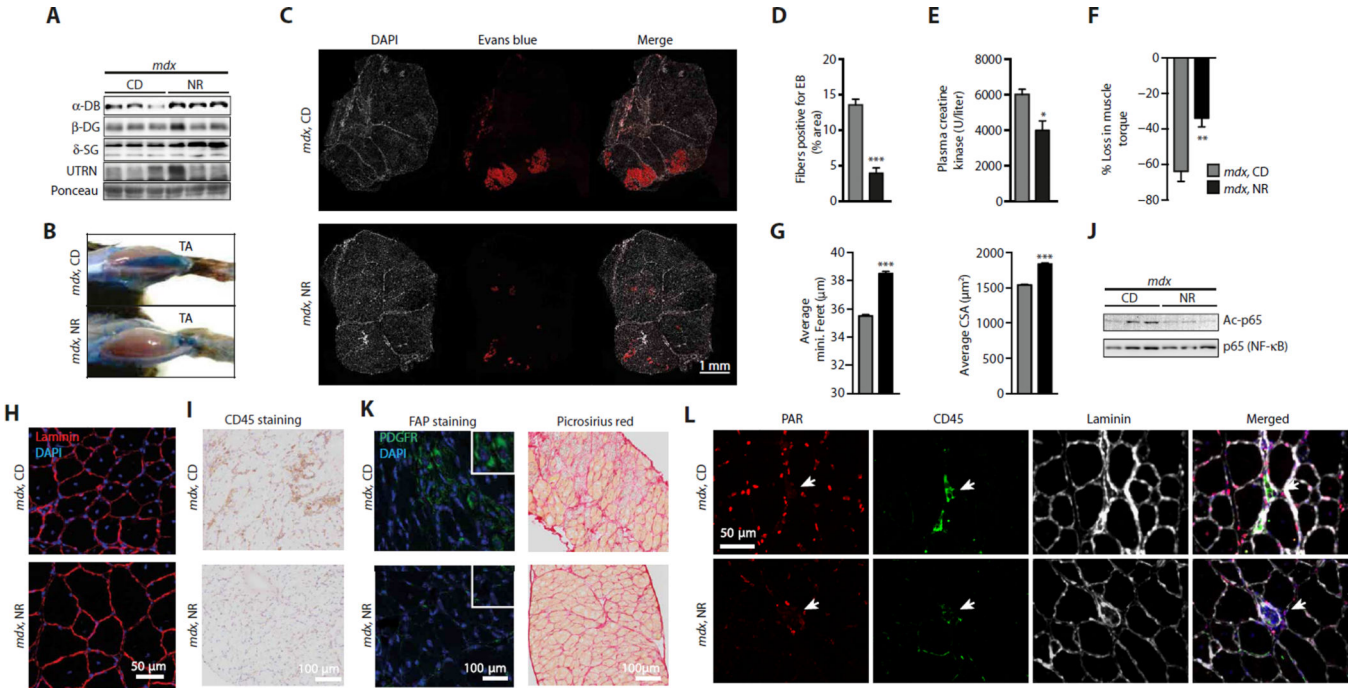

Fig. 5. NAD$^+$ repletion causes compensatory increases in the expression of structural proteins and protects muscle from damage and fibrosis

Sixteen-week-old *mdx* mice received a dietary supplement with NR (400 mg/kg per day) for 12 weeks. (**A**) NR-treated *mdx* mice exhibited increased α-dystrobrevin (α-DB) (CD, 1.00 ± 0.35; NR, 1.61 ± 0.09) and δ-sarcoglycan (δ-SG) (CD, 1.00 ± 0.15; NR, 2.24 ± 0.43; P = 0.026) protein expression compared to HSP90 (Fig. 4D) as a loading control in gastrocnemius extracts. NR attenuated *mdx* muscle damage as evidenced through (**B**) Evans Blue staining of both TA muscle and (**C**) sections of gastrocnemius and soleus muscles [red, Evans Blue (EB); white, 4′,6-diamidino-2-phenylindole (DAPI)], (**D**) quantified using ImageJ software (*mdx,* n = 6; *mdx* NR, n = 12). (**E**) NR also reduced basal plasma creatine kinase levels (*mdx,* n = 5; *mdx* NR, n = 6). (**F**) *mdx* mice treated with NR demonstrated an attenuation in the percent loss of torque in quadriceps, after muscle damage induced by lengthening contractions (*mdx,* n = 7; *mdx* NR, n = 6). (**G**) Increases in the average minimal Feret's diameter (in micrometers) and cross-sectional area (CSA) (in square micrometers) of tibialis anterior muscle fibers, indicating increases in fiber size with NR treatment in *mdx* mice. These data were acquired from images stained with DAPI and laminin [(**H**) shows a representative image]. Quantification of images was performed with ImageJ software (8 weeks of NR treatment, n = 5). (**I**) Similarly, reduced CD45 staining was seen in diaphragms of *mdx* mice treated with NR. (**J**) Reduced acetylation of p65 (NF-κB) protein after NR in quadriceps (CD, 1.00 ± 0.15; NR, 0.38 ± 0.16; P = 0.023; n = 3). (**K**) FAPs expressing mesenchymal PDGFRα were decreased in diaphragms of *mdx* mice treated with NR (n = 3). Also, reductions in the fibrosis of *mdx* diaphragms were observed with less Picrosirius red staining in transverse muscle sections of NR-treated mice. (**L**) PARylation intensity in skeletal muscle nuclei of *mdx* mice is reduced with NR, as shown with immunohistological staining of tibialis anterior muscle with PAR, CD45, and laminin antibodies.

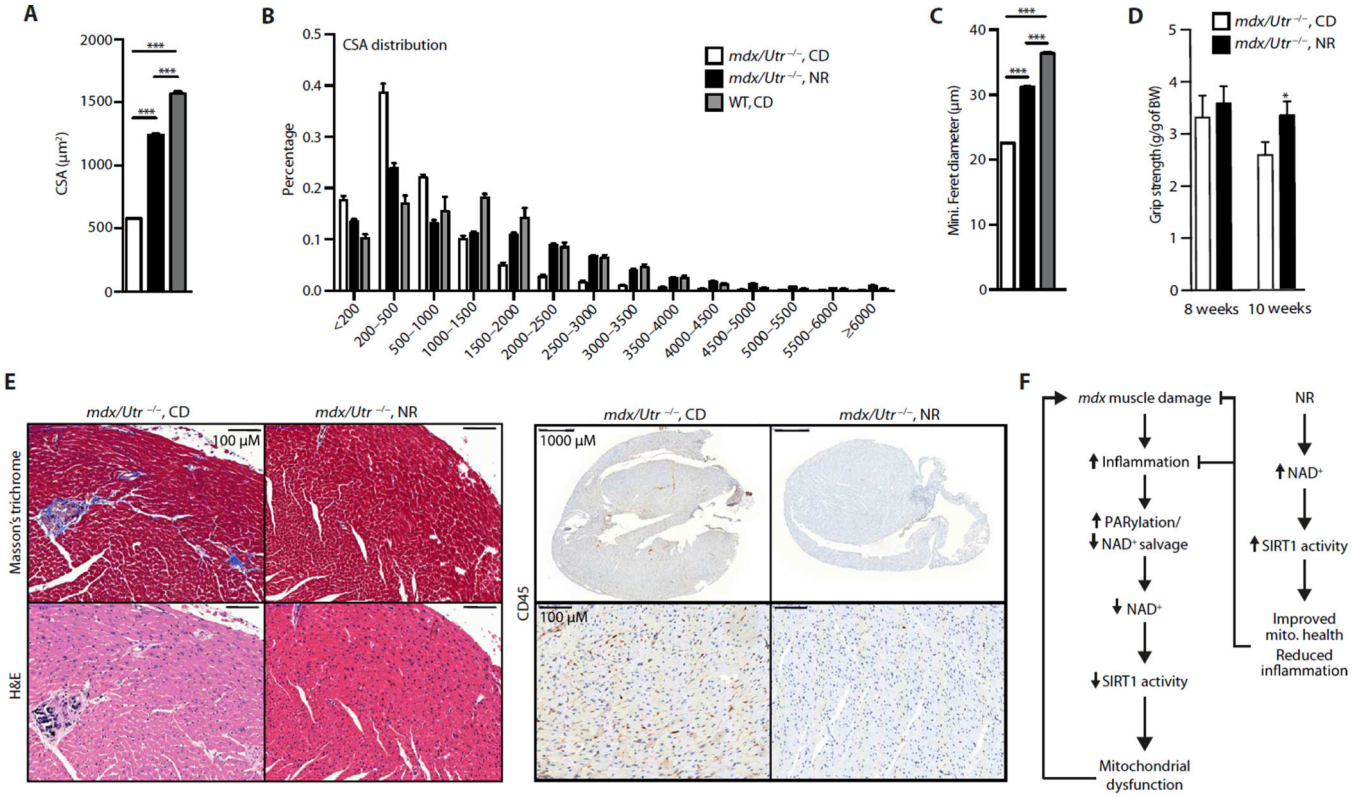

Fig. 6. *mdx/Utr*$^{-/-}$ mice recover skeletal muscle function and exhibit improved heart pathology with NR treatment

Three-week-old *mdx/Utr*$^{-/-}$ mice received a dietary supplement with NR (400 mg/kg per day) for 5 to 7 weeks. Images stained with DAPI and laminin were used to quantify increases in the (**A**) average and (**B**) distribution of *mdx/Utr*$^{-/-}$ mouse muscle fiber cross-sectional areas (in μm^2) of the tibialis anterior muscle (*mdx/Utr*$^{-/-}$ $n = 3$; 7 weeks of NR treatment). (**C**) NR-treated *mdx/Utr*$^{-/-}$ mice showed an increase in the minimal Feret's diameter (in micrometers) (*mdx/Utr*$^{-/-}$ $n = 3$; 7 weeks of NR treatment). Quantification of images was performed with ImageJ software. (**D**) As evidence for the therapeutic effectiveness of NR treatment, *mdx/Utr*$^{-/-}$ mice grip strength was improved from 8 weeks (*mdx/Utr*$^{-/-}$ $n = 4$; *mdx/Utr*$^{-/-}$ NR, $n = 7$; 5 weeks of NR treatment) to 10 weeks of age (*mdx/Utr*$^{-/-}$ $n = 3$; *mdx/Utr*$^{-/-}$ NR, $n = 5$; 7 weeks of NR treatment). BW, body weight. (**E**) Sections of heart tissue were (immuno) histochemically stained with Masson's trichrome, hematoxylin and eosin, and CD45, showing a reduction of cardiac fibrosis, necrosis, and macrophage infiltration, respectively, in the ventricles of *mdx/Utr*$^{-/-}$ mice at 4 weeks of age and treated with NR for 6 weeks (representative images from $n = 3$ *mdx/Utr*$^{-/-}$ and $n = 3$ *mdx/Utr*$^{-/-}$ NR). (**F**) Scheme summarizing the SIRT1-dependent effects of NR on *mdx* mouse muscle.